Palacký University Olomouc

Diploma Thesis

Olomouc 2022 **Martin Löffelmann**

Palacký University Olomouc

Faculty of Science

Department of Cell Biology and Genetics

Identification of new inhibitors of NPL4 protein and insight into the mechanism of their action

Diploma Thesis

Martin Löffelmann

Study Programme: Biology

Field of Study: Molecular and Cell Biology

Form of study: Full-time

Olomouc 2022

Supervisor: Mgr. Zdeněk Škrott, Ph.D.

Bibliographical identification

Name and surname of the author: Martin Löffelmann

Title: Identification of new inhibitors of NPL4 protein and insight into the mechanism of their action

Type of thesis: Diploma

Department: Department of Cell Biology and Genetics, Faculty of Science, Palacký University Olomouc

Supervisor: Mgr. Zdeněk Škrott, Ph.D.

Year of presentation: 2022

Abstract

Cancer cells are dependent on functional protein degradation systems due to an excess of mutated or incorrectly folded proteins. p97 pathway is one of these degradation systems and cooperates with the ubiquitin-proteasome system. Nuclear protein localization homolog 4 (NPL4) is one of key p97 cofactors and its inhibition by CuET results in NPL4 aggregation and heat shock response. This thesis focuses on NPL4 inhibition by dithiocarbamate-copper complexes and its mechanism. Dithiocarbamates (DTCs) easily form complexes with metals and are used in many fields such as agriculture or anti-alcoholism therapy. A screening of twelve complexes composed of the effect on NPL4, and cytotoxicity was performed, and resulted in a positive correlation. Six of twelve tested DTC-copper complexes showed both cytotoxicity and effect on NPL4. To confirm the DTC-copper interaction with NPL4, Drug affinity responsive target stability (DARTS) method was used on an isolated and purified NPL4. In addition, a synergy of copper and DTC-copper complexes was observed that enhanced the antitumour effect through NPL4.

Keywords: NPL4, CuET, dithiocarbamates, anticancer therapy, DARTS, synergy

Number of pages: 61

Number of appendices: 0

Language: English

Bibliografické údaje

Jméno a příjmení autora: Martin Löffelmann

Název práce: Identifikace nových inhibitorů proteinu NPL4 a vhled do mechanismu jejich účinku

Typ práce: Diplomová

Pracoviště: Katedra buněčné biologie a genetiky, PřF UP v Olomouci

Vedoucí práce: Mgr. Zdeněk Škrott, Ph.D.

Rok obhajoby práce: 2022

Abstrakt

Nádorové buňky jsou závislé na funkčních systémech proteinové degradace kvůli nadbytku mutovaných nebo nesprávně složených proteinů. Dráha p97 je jedním z degradačních systémů a spolupracuje s ubikvitin-proteasomovým systémem. Nuclear protein localization homolog 4 (NPL4) je jedním z klíčových kofaktorů p97 a jeho inhibice pomocí CuET vede k tvorbě NPL4 agregátů a spuštění heat shock response. Tato práce je zaměřena na inhibici NPL4 pomocí komplexů mědi a dithiokarbamátů a její mechanismus. Dithiokarbamáty (DTC) snadno tvoří komplexy s kovy a jsou používány v mnoha oblastech jako je zemědělství nebo léčba alkoholismu. Byl proveden skríning dvanácti komplexů složený z efektivity vůči NPL4 a cytotoxicity a jeho výsledkem byla pozitivní korelace. Šest z dvanácti testovaných DTC komplexů s mědí vykazovaly jak cytotoxicitu, tak efekt vůči NPL4. Pro potvrzení interakce NPL4 s komplexy DTC s mědí byla použita metoda Drug affinity responsive target stability (DARTS) na izolovaném a purifikovaném proteinu NPL4. Navíc byla pozorována synergie mezi mědí a komplexy DTC s mědí, která zesílila protinádorový efekt skrze NPL4.

Klíčová slova: NPL4, CuET, dithiokarbamáty, protinádorová terapie, DARTS, synergie

Počet stran: 61

Počet příloh: 0

Jazyk: angličtina

Declaration

I hereby declare that I elaborated this diploma thesis independently under the supervision of Mgr. Zdeněk Škrott, Ph.D. using information sources referred in the References chapter only. This thesis was elaborated at the Department of Cell Biology and Genetics.

…….

Martin Löffelmann

ACKNOWLEDGMENT

I would like to thank my supervisor Mgr. Zdeněk Škrott, Ph.D. for his guidance, patience, and all theoretical and practical skills that I could learn from him. I am also very grateful to Mgr. Martin Mistrík, Ph.D. for allowing me to work in his laboratory. I would also like to thank my wife and my family for their support.

This Diploma Thesis was supported by the Internal Grant Agency of Palacký University IGA_LF_2022_038.

Table of Contents

List of abbreviations

ADAM	A Disintegrin and metalloproteinase
ALS	Amyotrophic lateral sclerosis
AMPK	AMP-activated protein kinase
ATR	Ataxia telangiectasia and Rad3 related kinase
CuET	bis(diethyldithiocarbamate)-copper(II)
DMSO	Dimethylsulphoxide
DR5	Death receptor 5
DSF	Disulfiram
DTC	Dithiocarbamate
EFSA	European food safety agency
ERAD	Endoplasmic reticulum associated degradation
FDA	Food and Drug Administration
HIV	Human immunodeficiency virus
HSF	Heat shock transcription factor
HSP	Heat shock protein
MERS-CoV	Middle East respiratory syndrome coronavirus
MM	Multiple myeloma
mTOR	Mammalian target of rapamycin
NF-κB	Nuclear factor-κB
NPL4	Nuclear protein localization homolog 4
p97	Protein p97
PTM	Posttranslational modification
SARS-CoV	Severe acute respiratory syndrome coronavirus
SOD	Superoxide dismutase
UBX	Ubiquitin-X domain
Ufd1	Ubiquitin fusion degradation 1
ULK1	Unc-51-like autophagy activating kinase 1
UPR	Unfolded protein response
UPS	Ubiquitin-proteasome system
VCP	Valosin-containing protein

List of figures

Figure 21: Flow cytometry assay confirms the involvement of NPL4 in CuET-copper synergy.

1 INTRODUCTION

This thesis focuses on the identification of new inhibitors of NPL4 protein. NPL4 is one of cofactors that are essential for p97 pathway, a major protein degradation system in the cell. NPL4 recognizes ubiquitinated substrates meant for degradation and helps with their extraction from membranes or organelles. Due to its importance, inhibition of NPL4 is a potential antitumour strategy since cancer cells are more dependent on proteostasis and are prone to proteotoxic stress. One NPL4 inhibitor is already known – CuET. A product of disulfiram metabolism which belongs to the chemical substances known as dithiocarbamates (DTCs). The mechanism of NPL4 inhibition is yet unknown and its clarification may be an extension of the use of DTCs as possible therapeutics in the fight against cancer.

2 AIMS OF THE THESIS

1. Summarize the knowledge about DTCs and p97/NPL4 and insight into the mechanism of action
2. Development of a cytometric assay to test the effect on NPL4
3. Screening of DTC-copper complexes
4. Testing of DTC-copper complexes cytotoxicity
5. *In vitro* reaction between purified NPL4 and DTC-copper complexes

3 THE CURRENT STATE OF KNOWLEDGE

3.1 Proteins and Diseases

Proteins are essential biopolymers with many important functions. They maintain cellular communication, immunity, transportation, catalyse chemical reactions and participate in the structure of the cells and a whole organism. Proteins vary in their concentration under specific physicochemical conditions that affect cells. Protein properties can be changed due to posttranslational modifications (PTMs) such as acetylation, phosphorylation, glycosylation, sumoylation etc. These modifications extend the number of possible protein forms even more. PTMs affect several protein functions, e.g., protein-protein interactions, cell-cell interactions, receptor activation, enzyme function and protein folding.

A correct protein conformation is especially important for its function. The proper conformation is encoded in the linear amino acid sequence of the polypeptide chain. The biologically active conformation is stable only under physiological conditions, therefore the folding process is sensitive to intrinsic and extrinsic factors that may cause errors and result in misfolded or aggregate states[1]. These misfolded or aggregated forms may cause severe neurodegenerative diseases, like Alzheimer´s disease, Parkinson´s disease, or Huntington´s disease. The aggregates are characterised by the presence of amyloid fibrils – highly organized β-strand-rich aggregates forming cross-β structures when β-strands of the polypeptides run perpendicular to the long axis of the fibrils[2]. During amyloidosis, large amounts of aggregates accumulate in specific tissues and may overload the chaperone system, which can result in proteotoxic stress and cell death[3]. For example, α-synuclein and tau proteins are associated with Parkinson´s and Alzheimer´s disease and impair the nervous system.

The newly synthesized proteins with short amino acid sequences can fold spontaneously but large proteins with a complex structure need assistance. The mechanism which is responsible for the correct folding is the molecular chaperone network. It secures the protein quality control, maintains proteins in their native states and even targets the misfolded proteins for degradation[4]. Primarily the heat shock proteins (Hsp) play an essential role under stress conditions, e.g., heat or oxidative stress. The most known chaperones are Hsp90s, Hsp70s and Hsp60s. Another part of the system are chaperonins, double ring-shaped chaperones that encapsulate proteins for folding. If the

environmental temperature increases, it may cause protein unfolding or aggregation. An increased Hsp expression is triggered by heat shock transcription factors (HSF), that bind to DNA and induce chaperone gene expression, thus preventing nonspecific aggregation[5,6]. However, an age-related decrease in chaperones and other proteostasis systems occurs and may lead to the accumulation of aggregates and cell death[7]. The reason for this decrease is still unknown.

The importance of proteins is also involved in one of the most important but also deadliest diseases – cancer. One of the hallmarks of cancer is genome instability[8]. It consists of an accumulation of mutations, defects in DNA damage repair mechanisms, aneuploidy[9] or even polyploidy in cancer cells[10]. Therefore, an excess of chromosomes results in an excess of expressed proteins. Because protein synthesis itself is an error-prone process, the large amounts of excessed proteins can be mutated or have a wrong conformation. Together with other conditions in cancer cells like hypoxia and oxidative stress these factors trigger proteotoxic stress in tumours[11]. This results in the cancer cells being more dependent on protein quality mechanisms, like the chaperones[12].

Overexpression of previously mentioned Hsps has been observed in solid tumours[13] and multiple myeloma[14]. Inhibitors of Hsp90 are being tested in clinical trials for many types of cancer[15]. The same goes for HSF1 which plays an important role in heat shock response but also in cancer cells where it induces genes different from heat shock response. These genes are mainly associated with energy metabolism, cell cycle signalling, apoptosis, cell adhesion and even metastasis[16]. HSF1 was named a ´guardian of proteostasis in cancer´ and is considered an oncogene while HSF2 is a potential tumour suppressor[17]. Overall, these findings suggest that the degradation of damaged or mutated proteins is essential for the physiological state of the cells and the maintenance of proteostasis.

3.2 Protein Degradation

3.2.1 Ubiquitin Proteasome System

One of the cellular systems which is responsible for protein degradation consists of a protease called proteasome and a small protein ubiquitin. The ubiquitin-proteasome system (UPS) is located in the cytoplasm and nucleus and is a fundamental element in maintaining proteostasis[12]. Ubiquitin is conjugated over its C terminus to lysine residues

in a substrate. This is done through a cascade of enzymes E1, E2 and E3. The substrate tagged with a ubiquitin chain then binds to ubiquitin receptors associated with the proteasome that link it for degradation (**Fig. 1**). Ubiquitin is recyclable and can be reused in the next reaction.

The 26S proteasome consists of a 20S core particle and a 19S regulatory particle. The core particle has a cylinder-like shape, and the inner section contains proteolytic active β sites[18]. The regulatory particle controls the entry of a substrate into the proteasome and guides it inside. It is located at the ends of the core particle and opens a channel within it. For proteins to enter the channel, they must be unfolded first. The process is done by AAA ATPases (unfoldases). These enzymes are called Rpt1-6 and use the energy from ATP hydrolysis to unfold substrates so that they can enter the channel of the core particle and undergo degradation[19]. The ubiquitin chain is removed from the substrate by deubiquitinating enzymes Rpn11, Ubp6 and Uch37[18].

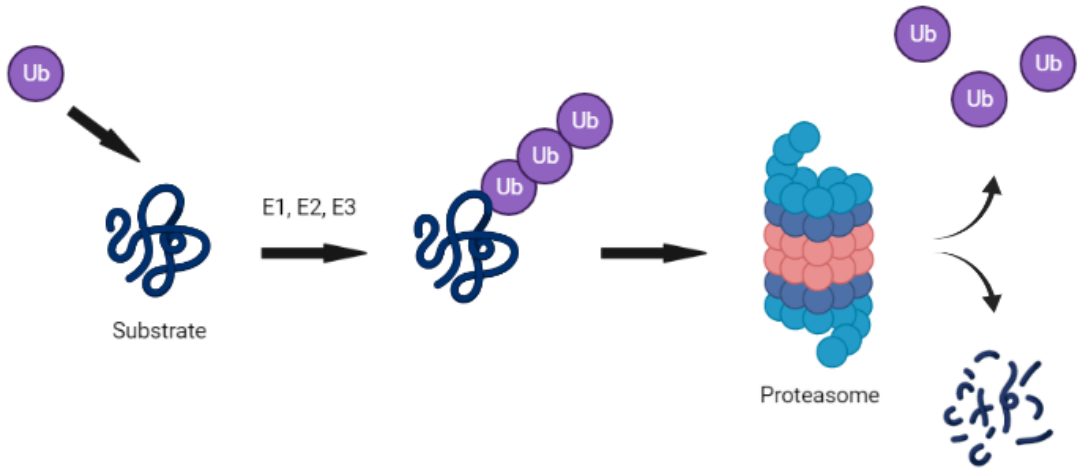

Figure 1: The Ubiquitin proteasome system. Ubiquitination of the target protein is done through E1, E2 and E3 enzymes on one or more lysine residues in a substrate. The ubiquitin chain then binds to ubiquitin receptors within the proteasome and links the substrate for degradation. Ubiquitin (purple) can be recycled for another reaction. *The figure was created in BioRender.com*

As mentioned above, cancer cells are more dependent on protein quality mechanisms and there is a risk of proteotoxic stress due to an excess of mutated or misfolded proteins[12]. Because of its essential role in maintaining proteostasis, the UPS became a target in anticancer therapy. Several proteasome inhibitors were synthesized and approved for clinical use. The approved first-generation proteasome inhibitor is bortezomib. It successfully inhibited the proteolytic sites in the UPS and caused

a cytotoxic effect in multiple myeloma (MM)[20] and non-Hodgkin´s lymphoma[21] in phase I and II clinical trials. Other proteasome inhibitors ixazomib and carfilzomib have also received an approval and are used in patients with MM or mantle cell lymphoma while oprozomib, marizomib and delanzomib are currently being tested in clinical trials[22] (**Fig. 2**).

However, the effect of proteasome inhibitors appears to be limited to MM or lymphomas. Bortezomib therapy showed minimal outcomes in solid tumours either administered alone or in combination with other agents[23]. Finally, as with other antitumour therapeutics, resistance to proteasome inhibitors has been identified[24,25]. Whether it is a natural resistance in solid tumours or an acquired one in MM and lymphomas, it represents a complication in therapy and raises questions about the mechanism.

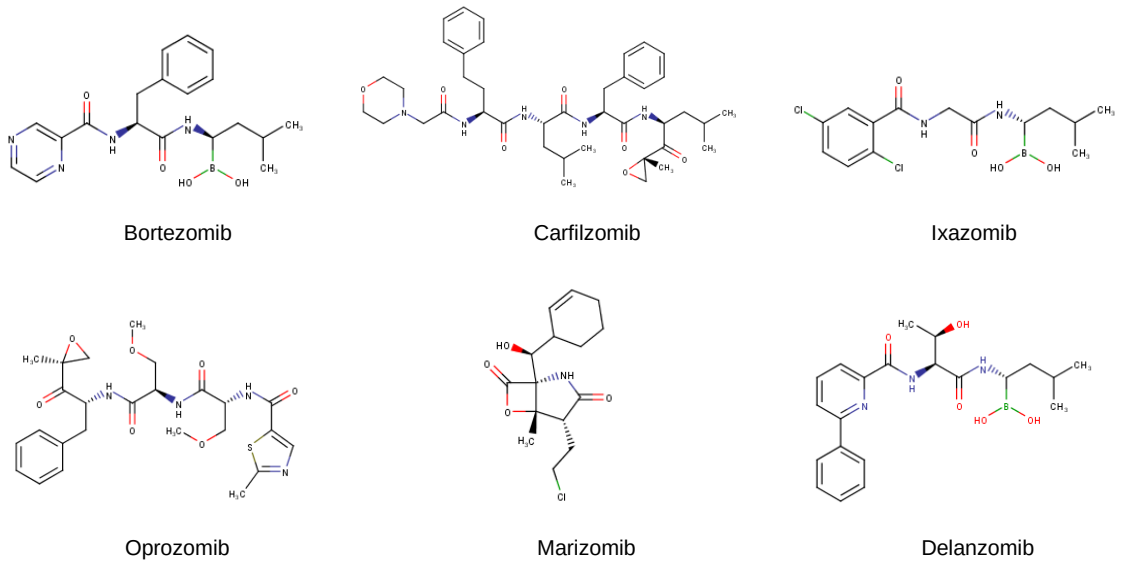

Figure 2: Structures of proteasome inhibitors. The upper substances have received an approval for clinical use. The lower ones are being tested in clinical trials. *Structures were created in MarvinSketch.*

3.2.2 Autophagy

While the UPS degrades intracellular proteins, autophagy is a pathway which involves the degradation of long-lived organelles (e.g., mitochondria, peroxisomes, or endoplasmic reticulum), microorganisms, lipid droplets and protein aggregates as well. Three forms of autophagy have been identified: macroautophagy, microautophagy and chaperone-mediated autophagy.

The principle of autophagy is that the cytosolic substrate is transported to the lysosome, where it is degraded by hydrolases. At first, the isolation membrane surrounds the substrate that is designated for degradation and then a double-membrane vesicle called an autophagosome is formed. The vesicle fuses with the lysosome and forms an autolysosome. Then the substrate is degraded together with the inner membrane[26].

The regulation of autophagy is done through several signalling pathways. The most important is the unc-51-like autophagy activating kinase 1 (ULK1), the phosphorylation of which determines the activation of autophagy. The Mammalian Target of Rapamycin (mTOR) kinase is a negative regulator of autophagy when it phosphorylates ULK1 under nutrient-rich conditions and stops the process. The positive regulator is AMP-activated protein kinase (AMPK). AMPK during nutrient depletion phosphorylates ULK1 and activates autophagy[27]. Therefore, both mTOR and AMPK combine nutritional factors and phosphorylation in the regulation. The formation of autophagosomes and other signalling pathways needed for the correct execution are conducted by Atg proteins[28].

As an important system for maintaining homeostasis, autophagy is associated with many diseases. Proteins degraded by the UPS need to be unfolded due to the narrow channel of the core particle. Nevertheless, autophagic degradation has lower requirements. Even aggregated proteins with polyglutamine expansions in Huntington´s disease[29] or mutant forms of α-synuclein in Parkinson´s disease[30] can be eliminated via autophagy. A strong correlation has been found between tumour suppressors and positive regulators of autophagy. For example, p53 promotes autophagy by inhibiting mTOR and activating AMPK in cancer cells[31]. A metabolic disbalance is a common feature in tumours, which can induce apoptosis. However, apoptotic pathways are inhibited in many tumours and autophagy supports cell survival in maintaining nutritional supply. Inhibition of autophagy in tumours with defect apoptosis during metabolic stress resulted in necrosis, which can trigger inflammatory response[32].

3.2.3 p97/VCP

p97 or Valosin-containing protein (VCP) is one of the key regulators of proteostasis and connects processes like the UPS, autophagy, cell cycle regulation and chromatin-associated functions. It belongs to the AAA ATPases family and uses energy from ATP hydrolysis to remodel target substrates. Also, its essential role is in endoplasmic reticulum-associated degradation (ERAD)[33].

p97 is a hexamer and the structure of each subunit contains two ATPase domains, D1 and D2, and six N-terminal domains. p97 associates with many cofactors that contain binding domains through which they can bind to N-domains of p97. The cofactors play an important role in the reactions in which p97 participates, for example, serve as ubiquitin adaptors. The major family of cofactors are proteins that contain a ubiquitin-X domain (UBX), or UBX-like domain[34]. Among the most important cofactors are Ubiquitin fusion degradation 1 (Ufd1), Nuclear protein localization homolog 4 (NPL4) or p47[35].

One of the p97 functions is to bind ubiquitinated proteins, remodel them structurally and help with their transportation from cellular complexes or membranes. This process happens especially during ERAD when the p97-Ufd1-NPL4 complex extracts the ubiquitinated substrate from the ER to cytosol and enables it for degradation in the proteasome[33] (**Fig. 3**).

The cell cycle regulation is another system where p97 plays its part. In HeLa cells, Ufd1-NPL4 cofactors are required for correct chromosome segregation during mitosis. In addition, NPL4 alone can partially fulfil the function of the complex in the case of Ufd1 depletion. Also, depletion of Ufd1-NPL4 resulted in increased levels of Aurora B kinase[36], which is necessary for the proper mitotic spindle attachment to the kinetochore. This finding indicates that p97 antagonizes Aurora B and affects its kinase activity[33].

p97 is associated with a broad spectrum of diseases due to its broad spectrum of cellular functions. Increased levels of p97 in prostate, gastric, colorectal or pancreatic cancer correlate with metastasis and poor prognosis[37]. There is a connection between p97 and a rare autosomal dominant disease called Inclusion body myopathy associated with Paget disease of bone due to the missense mutations in the gene encoding p97[38]. Moreover some mutations were present in 1-2% of amyotrophic lateral sclerosis (ALS) cases[39].

Because of the various and important roles of p97 in cells, it is not surprising, that it became a target in therapy. CB-5083 is a promising selective inhibitor of p97 with antitumour activity. Inhibition of p97 results in an accumulation of misfolded proteins in the ER and triggers the unfolded protein response (UPR)[40]. The UPR upregulates a death receptor 5 (DR5) that activates apoptosis via caspase-8 and caspase-3/7[41]. Another interesting feature of CB-5083 is its efficacy against solid tumours in contrast with bortezomib and other proteasome inhibitors[42]. These features and results were put to test in phase I clinical trials in multiple myeloma[43] and advanced solid tumours[44]. Unfortunately the clinical trials were prematurely terminated due to an effect on off-target

which was phosphodiesterase-6 that caused visual loss in patients[45]. On the other hand bortezomib also showed antitumour activity in solid tumours in mice[46].

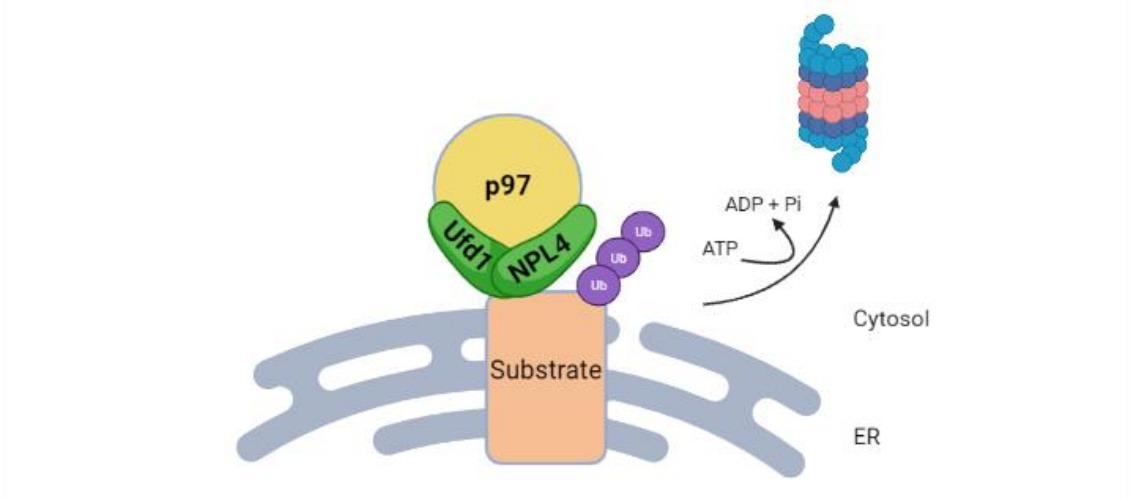

Figure 3: p97-Ufd1-NPL4 complex and ERAD. The complex facilitates the extraction of the target substrate which is ubiquitinated on the cytosolic side, from the ER and makes it available for degradation by the proteasome. p97 binds to the substrate through its cofactors. *The figure was created in Biorender.com*

3.2.3.1 NPL4 Protein

NPL4 (also known as NPLOC4) as mentioned above is one of the p97 cofactors that is responsible for recognition of polyubiquitinated substrates. It forms a heterodimer with Ufd1 and together participate in the extraction of ubiquitinated substrates during ERAD. NPL4 consists of several domains: UBX-like domain, two zinc finger domains, Mrp1/Pad1 N-terminal (MPN) domain, C-terminal domain and NPL4 zinc finger (NZF) domain. The latter serves to bind NPL4 to the ubiquitinated substrate[47].

The X-ray structure of NPL4 alone is not yet available, only with a bound complex of Ufd1 and diubiquitined Lys48 which revealed that MPN domain is important for the binding to Ufd1[47]. A cryo-electron microscopy structure of NPL4/Ufd1/p97 complex from *Chaetomium thermophilum* showed that NPL4 interacts through its UBX-like domain with the N-domain of p97 and uses its two zing finger domains to anchor the MPN domain to the D1 which is an ATPase domain of p97[48]. The instability of the protein itself seems to make it very difficult to obtain its structure without binding partners.

A higher expression of NPL4 was observed in renal cell carcinoma[49] and bladder cancer[50] and is associated with poor prognosis. This information together with the fact

that its inhibition would have a major impact on proteostasis make NPL4 a possible target for anticancer therapy.

3.3 Dithiocarbamates as Potential Therapeutics

3.3.1 Applications of Dithiocarbamates

Dithiocarbamates (DTCs), or carbamodithioates, are small organic compounds that are easily synthesized and have a wide range of applications. Structurally, it is a class of monoanionic 1,1-dithio ligands (R2CNS-2). The DTCs have two polarization states. The first one is a balanced stage, in which a double bond is formed between a carbon and sulphur. A negative charge occurs on the second sulphur, which makes it capable of interactions with other compounds, including metals. The second resonance stage has a decentralization between the two sulphurs[51] (**Fig. 4**). Most DTCs are stable in neutral and basic pH, however, they decompose under acidic conditions.

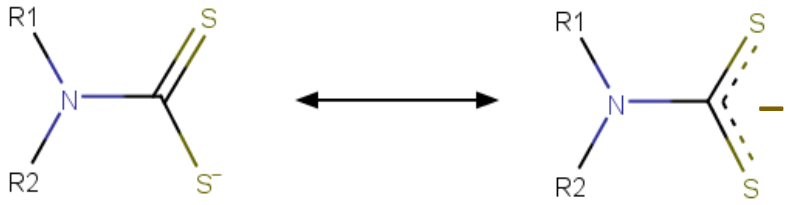

Figure 4: Structure of dithiocarbamates. DTCs may have two polarization states. *Structures were created in MarvinSketch.*

One of the main features of DTCs is their chelating activity and ability to form complexes with a diverse group of metals, such as copper, iron, nickel, gold and ruthenium[52]. This activity has biological consequences because it can destabilize the structure of proteins or enzymes that have these metals in their centre or act as cofactors in various biochemical processes. A lack of these cofactors can inhibit essential signalling pathways and have serious consequences for cell viability. In addition, the chelating activity acts as an antidote to metal poisoning[53].

DTCs have been used as antiprotozoal, anthelmintic, and antiviral agents. A recent evaluation indicated their possible use as new drugs against *Trypanosoma cruzi*, which is

a protozoan responsible for Chagas disease. Another possible therapeutic use from this evaluation was against leishmaniasis and African trypanosomiasis[51]. Thanks to simple synthesis, DTCs could represent a major advance in the treatment of tropical diseases in developing countries.

Another application of DTCs is in agriculture as fungicides and pesticides. The fungicidal activity of DTCs is known since the 1940s and the compounds used in various crops are propineb, zineb, maneb, thiram and mancozeb[54]. Such a long period of use requires specific methods for detecting these substances in food. This was emphasized by the European Food Safety Agency EFSA in its report in 2017[55] with regard to the health of consumers.

In general, DTCs are being repurposed in various therapies. Their effects have been addressed in many fields over the past 20 years, including cardiology, neurology, and oncology. Antiviral activity against Human immunodeficiency virus (HIV)-1 has also been reported and clinical trials are underway[56]. In the centre of these repurposing strategies and clinical trials is one specific compound which is disulfiram.

3.3.2 Disulfiram

Disulfiram (DSF) is an oxidized form of dithiocarbamate (**Fig. 5A**). Other names are Antabuse or Tetraethylthiuram disulphide. It was originally developed in the 19th century for the rubber industry. The first therapeutic use was in the 1930s as a vermicide and a scabiescide, due to its copper chelating activity which disrupted the respiratory enzymes of the parasites[57]. The most known use of DSF is as an anti-alcoholism drug under the name Antabuse. The mechanism of action in aversion therapy is the irreversible inhibition of liver aldehyde dehydrogenase (ALDH), which results in the accumulation of acetaldehyde in blood after alcohol consumption[58]. That leads to a toxic reaction with symptoms like sweating, blurred vision, nausea, vomiting, hyperventilation, anxiety and may even result in a cardiovascular collapse. The aversive reaction may take from several hours for up to two weeks until the required amount of unbound enzyme is synthesized for alcohol metabolism[59].

Disulfiram, like DTCs, is unstable under acidic conditions. When DSF is orally administered and enters the digestive tract, it is converted to a metabolite diethyldithiocarbamate that is further metabolised to other compounds including S-methyl-N,N-diethylthiocarbamate sulphoxide and S-methyl-N,N-diethylthiocarbamate sulphone. These two metabolites were suggested to inhibit ALDH[60,61]. Diethyl-DTC

easily forms complexes with metals, especially copper[62]. Copper ions (II) from blood and urine together with diethyl-DTC form a complex called CuET – bis(diethyldithiocarbamate)-copper(II) (**Fig. 5B**). CuET is insoluble in water but soluble in DMSO and other organic solvents where it forms a dark brown solution. This feature indicates the lipophilicity of the substance and its possible penetration into cells across the cytoplasmic membrane and a role as an ionophore[63].

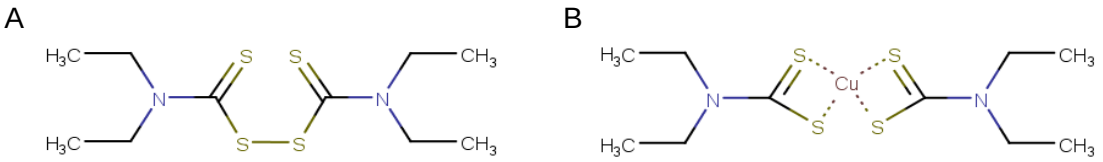

Figure 5: Structures of disulfiram (**A**) and CuET (**B**). CuET is a dithiocarbamate-copper complex and a metabolic product of disulfiram. *Structures were created in MarvinSketch.*

DSF is receiving an attention in antitumor therapy. This is supported by 22 clinical trials (clinicaltrials.gov) conducted as of April 2022 with DSF in cancer. Early studies have focused on the effect on superoxide dismutase (SOD)[64] when the activity of the enzyme was impaired due to DSF copper chelating activity. Another reported mechanism was the inhibition of NF-κB transcription factor[65,66]. This signalling cascade is necessary for the proper functioning of the immune system. It regulates the expression of signalling molecules like cytokines, growth factors, and is involved in apoptosis and cell proliferation. Therefore it is not surprising that unregulated NF-κB activation may contribute to malignancies and is a target in anticancer therapy[67].

Because of the metabolic disbalance in cancer cells and high concentration of copper[68] CuET is easily and spontaneously formed. And CuET appears to be the key molecule with antitumour activity. There are several published articles regarding the mechanism of action of CuET in cancer cells[69,70].

One hypothesis about the CuET mechanism is a proteasome inhibition[71]. However, this hypothesis was clarified that not the proteasome, but one of the p97 cofactors – NPL4 protein is inhibited[69,70]. In case of p97 malfunction when ubiquitinated proteins accumulate in the cell, the UPS does not work properly either. However, the target is NPL4 protein itself because after CuET treatment, NPL4 aggregates were observed in cells. The aggregation is possible due to the presence of two zinc-finger

domains in NPL4 that can bind bivalent metals. These aggregates trigger a heat shock response that mobilizes Hsps[69]. A recent study showed the antitumour activity of CuET with NPL4 immobilisation even in resistant MM cells against proteasome inhibitors bortezomib and carfilzomib[72]. In addition, CuET also induces DNA damage and at the same time impairs the DNA damage repair mechanism ATR kinase[73].

This thesis is focused on NPL4 inhibitors and their mechanism of action in cancer cells. Given the much evidence of efficacy associated with the effect on NPL4, it is clear that this is a path worth exploring further.

DSF has become a promising compound also in other therapeutic areas. A screening of 640 FDA-approved drugs was performed to find a suitable substance for the treatment of Alzheimer´s disease. DSF was identified as a very promising candidate. It increased the gene expression of ADAM10, which is a metalloproteinase that prevents formation of the amyloidogenic β-strand-rich polypeptides, one of the hallmarks of Alzheimer´s disease. This activity was confirmed in mouse models as well[74]. Antiviral activity of DSF was observed due to its inhibition of papain-like proteases of coronaviruses SARS-CoV and MERS-CoV[75]. The protease is essential for the cleavage of viral polyproteins that are translated after infection of a cell and the suppression of the host immune system because of a block in NF-κB pathway[76]. In search of effective anti-SARS-CoV-2 treatment, DSF and ebselen in combination with remdesivir resulted in synergy and inhibition of the viral proofreading activity and viral replication and translation[77].

Well-known compounds like DSF and DTCs may have many unknown positive effects against diseases that we sometimes struggle to treat and overcome. Since DSF is administered orally, is readily available, inexpensive, and has many applications in various therapies, these facts indicate its hidden potential. The same goes for other substances that have been used for specific purposes for decades, however, their effect may be several times higher in areas where they have never been tested. We should keep in mind that even old and simple molecules can have the answers we are looking for.

4 MATERIALS AND METHODS

4.1 Materials

4.1.1 Biological material

- U2OS – Organism: *Homo sapiens*, human; Tissue: bone; Disease: osteosarcoma; Culture Properties: adherent; Morphology: epithelial; ATCC® HTB-96™
- U2OS-NPL4-GFP genetically modified cell line created and described in ref[69]
- H1299 – Organism: *Homo sapiens*, human; Tissue: lung; Disease: non-small cell lung carcinoma; Culture Properties: adherent; Morphology: epithelial; ATCC® CRL-5803™
- Genetically modified bacteria *E. coli* BL21 (DE3) NPL4-GST (Novagen) created and described in ref[69]
- NPLOC4-GFP, pCMV6-AC-GFP vector (NM_017921, Origene)

4.1.2 List of equipment, chemicals and machines

List of equipment

- Automatic pipettes, Research Plus (0,5–1 000 µl, Eppendorf, Discovery)
- Battery-powered pipette filler, Swiftpet Pro (HTL)
- Bio-Scale™ Mini, Profinity™, GST Cartridge 5 ml (Biorad)
- Cell scrapers (TPP)
- Centrifugal Filters and Tubes for DNA and protein purification and concentration, Amicon® Ultra 0.5ml incl Ultracel 30K membrane (Merck)
- Centrifuge tubes (15 ml, 50 ml, TPP)
- Desalting column, HiTrap™ (5 ml, GE Healthcare)
- Eppendorf Safe-Lock Tubes (1.5-2 ml, Eppendorf)
- Erlenmeyer flasks, wide neck (250 ml, Simax)
- Glass bottles (250-1 000 ml, Fisherbrand)
- Microscope slides, Superfrost™ Plus (Thermo Fisher Scientific)
- Microscope cover glasses circular (diameter 15 mm, Paul Marienfeld GmbH & Co. KG)
- Nitrile gloves (Vulcan)
- Nitrocellulose Membrane (0.45 µm, Biorad)
- Protein Electrophoresis Equipment (Biorad)

- Serological pipettes, sterile (5-25 ml, SPL)
- Test flow cytometry tubes (5 ml, BD Falcon)
- Tissue culture dishes (60x16 mm, growth surface 22 cm^2, TPP)
- Tissue culture flasks (25, 75 cm^2 growth surface, TPP)
- Tissue culture test plates (6, 12, 96-well, TPP)
- Vacuum Desiccator (Simax)

List of chemicals

- 10X PBS
- 30% Acrylamide/Bis Solution, 29:1 (1610156, Biorad)
- 70% Ethanol
- 4% Formaldehyde solution (HT501128, Sigma-Aldrich)
- 100% Methanol
- Acetic acid 99% (Penta)
- Ammonium persulphate, reagent grade, 98% (215589, Sigma-Aldrich)
- Ampicillin (59349, Sigma-Aldrich)
- Bovine Serum Albumin (BSA), heat shock fraction, pH 7, ≥ 98% (A7906, Sigma-Aldrich)
- Brilliant Blue R, pure (B7920, Sigma-Aldrich)
- Bromophenol Blue, ACS reagent (114391, Sigma-Aldrich)
- Cadmium chloride, technical grade (655198, Sigma-Aldrich)
- Copper (II) chloride dihydrate, ACS reagent (307483, Sigma-Aldrich)
- DAPI, for nucleic acid staining (D9542, Sigma-Aldrich)
- Dimethyl sulphoxide (DMSO) Cell culture grade (APA3672.0250, PanReac AppliChem)
- Di-sodium Hydrogen Phosphate Dodecahydrate, G.R. (Lach-Ner)
- DL-Dithiothreitol (DTT), ≥ 98% HPLC (D0632, Sigma-Aldrich)
- DMEM High Glucose Medium w/ Stable Glutamine, w/ Sodium Pyruvate, sterile filtered, (LM-D1110, Biosera)
- Ethylenediaminetetraacetic acid disodium salt dihydrate (EDTA), suitable for electrophoresis, for molecular biology, (E5134, Sigma-Aldrich)
- Fetal Bovine Serum (FBS), Gibco™, (10270106, Thermo Fisher Scientific)

- G 418 disulphate salt (A1720, Sigma-Aldrich)
- Glycerol anhydrous, A.G. (14550-11000PE, Penta)
- Glycine, suitable for electrophoresis, ≥ 99% (G8898, Sigma-Aldrich)
- Iron(III) chloride, reagent grade, 97% (157740, Sigma-Aldrich)
- Isopropyl β-D-thiogalactopyranoside (IPTG), Invitrogen™ (15529019, Thermo Fisher Scientific)
- LB medium for bacterial culture
- L-Glutathione reduced, ≥ 98% (G4251, Sigma-Aldrich)
- Penicillin-Streptomycin (P/S), (P4333, Sigma-Aldrich)
- Phenylmethylsulphonyl chloride (PMSF) (Sigma-Aldrich)
- Potassium Dihydrogen Phosphate (30016, Lach-Ner)
- Precision Plus Protein™ Standard Dual Color (1610374, Biorad)
- Pronase from *Streptomyces griseus* (10165921001, Roche)
- Purified water
- SilverQuest™ Silver Staining Kit (Thermo Fisher Scientific)
- Skimmed Milk Powder (Samantha)
- Sodium chloride, puriss. p. a., ACS reagent grade, ≥ 99,5% (31434-M, Sigma-Aldrich)
- Sodium dihydrogenphosphate dihydrate, p.a. (12340-31000, Penta)
- Sodium dodecyl sulphate (SDS), ≥ 98.0% GC (71729, Sigma-Aldrich)
- Sodium Silicate (aqueous solution)
- SuperSignal™ West Pico Plus Chemiluminescent Substrate (Thermo Fisher Scientific)
- TEMED (N,N,N′,N′- tetramethyl ethylenediamine), (T9281, Sigma-Aldrich)
- Transfection reagents Viromer® RED (Lipocalyx)
- Tris(hydroxymethyl)aminomethane (37180.04, Serva)
- Triton X-100 (3051.2, Roth)
- Trypsin TrypLE™ Express Enzyme (1X) incl phenol red (12605028, Thermo Fisher Scientific)
- Tween 20, Catalog No. 103168 (MP Biomedicals)
- Vectashield® Mounting Medium (H-1000, Vector Laboratories)

- XTT activator – Phenazine methosulphate (P9625, Sigma-Aldrich) dissolved in water, 0.38 mg/ml
- XTT reagent – XTT sodium salt Biochemica (A2240, PanReac AppliChem) dissolved in RPMI-1640 Medium w/o phenol red, 0.9 mg/ml (R7509, Sigma-Aldrich)
- Zinc sulphate heptahydrate, *ReagentPlus*®, ≥ 99.0% (Z4750, Sigma-Aldrich)

List of antibodies

Primary antibodies

- β-Actin (C4), mouse monoclonal IgG, Catalog No. sc-47778 (Santa Cruz Biotechnology); dilution factor 1:500
- NPL4 Antibody (D-1), mouse, monoclonal, Catalog No. sc-365796 (Santa Cruz Biotechnology); dilution factor 1:500
- NPLOC4 Antibody, rabbit, polyclonal, Catalog No. NBP1-82166 (Novus Biologicals); dilution factor 1:1 000

Secondary antibodies

- Sheep Anti-Mouse IgG – Horseradish peroxidase, Catalog No. NA931V (GE Healthcare); dilution factor 1:1 000
- Donkey Anti-Rabbit, Catalog No. NA934V (GE Healthcare); dilution factor 1:1 000

List of machines

- Analytical balances, BBI-32 (Boeco)
- Cell Viability Analyzer Vi-Cell XR (Beckman Coulter)
- Centrifuge, 420R Rotina (Hettich)
- ChemiDoc Universal Hood III (Biorad)
- Dry Bath Incubator (Major Science)
- Flow cytometer, BD Facs Verse (BD Life Sciences)
- FPLC-NGC Chromatography System (Biorad) incl Fraction Collector-BioFrac (Biorad)
- Incubator, HERA Cell 150i CO2 incubator (Thermo Fisher Scientific)
- Laminar box, MSC Advantage (Thermo Fisher Scientific)

- Laser Scanning Confocal Microscope, LSM 780 (Zeiss)
- Light Microscope, Primovert (Zeiss)
- Magnetic Stirrer, MSH-300i (Biosan)
- Orbital Shaking Platform, PSU-10i (Grant Instruments)
- pH Meter, HI-2211 (Hanna Instruments)
- Plate reader, Infinite® 200 Pro (Tecan)
- PowerPac™ HC High-Current Power Supply (Biorad)
- Shaker/incubator, KS-15 control (Edmund Bühler)
- Shaker/incubator, KS 4000i control (IKA)
- Trans-Blot® SD Semi-Dry Transfer Cell (Biorad)
- Ultrasonic Cleaner, USC-THD (VWR)
- Ultrasonic Homogenizer, Sonopuls, UW Mini 20 (Bandelin)
- Ultraviolet Crosslinker, CL-1 000 (UVP)
- Vortex-Genie 2 (Scientific Industries)
- Waterbath, WNB (Memmert)

4.1.3 List of solutions

Solutions and media for cell culture

1X PBS: 450 ml purified water + 50 ml 10X PBS

DMEM complete medium (10% FBS, 1% P/S): 500 ml DMEM High Glucose w/ Stable Glutamine, w/ Sodium Pyruvate + 50 ml FBS + 5 ml P/S

Drug Affinity Responsive Target Stability

Phosphate buffer: dissolve 100 mM $NaH_2PO_4 \cdot 2H_2O$ and 100 mM $Na_2HPO_4 \cdot 12H_2O$ in 50 ml of H_2O, adjust pH to 7.4, store at 4 °C

Pronase concentrated solution: dissolve 1 mg of Pronase in 1 ml of TNC buffer

TNC buffer: dissolve 50 mM NaCl, 50 mM Tris and 10 mM $CaCl_2$ in 50 ml of H_2O, adjust pH to 7.5, store at 4 °C

DTC-copper complexes

100 mM DTCs dissolved in water were mixed with 100 mM $CuCl_2$ in a ratio of 2:1 in DMSO to the concentration of 1 mM.

Twelve DTCs were used in the experiments. Eight DTCs were purchased from different companies and four were synthesized by a collaborating laboratory. Tested DTC-copper complexes were numbered from one to eleven due to the patent protection of certain substances. CuET was the twelvth compound and, in addition, was used as a positive control in various experiments such as the development of a flow cytometric assay, DARTS and others.

Isolation and purification of NPL4 protein

10X PBS: dissolve 1.4 M NaCl, 27 mM KCl, 100 mM $Na_2HPO_4 \cdot H_2O$ and 18 mM KH_2PO_4 in 1 000 ml of H_2O, adjust pH to 7.3; dilute to 1X before use

20% EtOH: filter and degas the solution before use

Bacterial cell lysis buffer: mix 50 ml of 150 mM NaCl with 50 ml of 1X PBS and add 1 ml of 10% Triton

Elution buffer for GST cartridge: dissolve 100 mM Tris and 5 mM EDTA in 1 000 ml of H_2O, adjust pH to 8.0; before use add glutathione to a final concentration of 20 mM

Phosphate buffer: dissolve 100 mM $Na_2HPO_4 \cdot 12H_2O$, 100 mM $NaH_2PO_4 \cdot 2H_2O$ in 500 ml of H_2O. Add H_2O to 1 litre and add 150 mM NaCl, adjust pH to 7.5, filter and degas the solution before use

Purified water: filter and degas the solution before use

SDS-PAGE and Western blotting

4X Laemmli Sample Buffer (LSB): 40% glycerol, 240 mM Tris-HCl pH 6.8, 8% SDS, 0.04% bromophenol blue. Separately was prepared 1 M DTT, which was diluted into the LSB 6 times.

10X Running buffer: dissolve 30 g of Tris, 144 g of Glycine and 10 g of SDS in 1 000 ml of H_2O. Dilute to 1X before use.

10X Transfer buffer: dissolve 30 g of Tris and 144 g of Glycine in 1 000 ml of H_2O. Preparing 1X solution – mix 800 ml H_2O + 100 ml MeOH + 100 ml 10X Transfer Buffer

10X TBS: dissolve 24 g of Tris, 88 g of NaCl in 1 000 ml of H_2O, adjust pH to 7.6 Dilute to 1X before use.

5% milk in TBS-Tween: dissolve 2.5 g of skimmed milk powder in 50 ml of TBS-Tween

Coomassie blue staining: 50% MeOH, 10% Acetic acid, 0.1% Brilliant Blue R, 40% H_2O

Destaining solution: mix 50 ml of MeOH with 50 ml of H_2O

TBS-Tween: add 1 ml of Tween 20 per litre of 1X TBS

XTT assay

XTT complete solution: XTT Reagent 10 ml + XTT Activator 200 µl

4.2 Methods

4.2.1 Microscopy of NPL4 aggregates

For the microscopy analysis, the U2OS-NPL4-GFP cells were seeded in a 12-well plate. Before seeding a set of small circular plastic discs, with a diameter of 18 mm each, was put into the Crosslinker under UV, with the settings 2 000 x 100 µJ/cm^2. After that one disc was placed in each well of the 12-well plate. The cells were seeded 100 x 10^3 cells/well in 2 ml of a complete medium.

After 24 hours of incubation, the cells were treated. Two wells were selected for a fixation procedure and the other two wells for a pre-extraction. Each set contained a control, which was 0.5% DMSO and the treated wells with 1 µM CuET. The plate was put into the incubator for three hours.

After incubation, the fixation set was prepared under non-sterile conditions. The medium was removed, and the cells were washed with 1X PBS. 1 ml of 4°C, 4% formaldehyde was added to each well. Incubation for 15 min, room temperature (RT) in dark. The formaldehyde was removed, and the cells were washed with 1X PBS.

The pre-extraction set was prepared under non-sterile conditions as well. After incubation, the medium was removed, and the cells were washed with 1X PBS. 1 ml of 0.2% Triton in 1X PBS was added to the cells for one minute. The Triton in PBS was removed and 1 ml of 4°C, 4% formaldehyde was added to the cells. Incubation for 15 min, room temperature (RT) in dark. The formaldehyde was removed, and the cells were washed with 1X PBS.

The 1X PBS was removed from both sets and 1 ml of 0.2% Triton in 1X PBS was added to all wells for two minutes. Afterwards, the Triton was removed, the cells were washed with 1X PBS and 1 ml of 1µg/ml DAPI was added. Incubation for two minutes, RT in dark. The DAPI was removed, the cells were washed with purified water and left

to dry out in dark at RT. Then 45 µl of sodium silicate (aqueous solution) were pipetted onto a microscope slide, on which the circular plastic disc containing the cells was placed. 2 µl of a mounting medium was put on a plastic disc, on which a circular cover glass was placed. The microscopy was performed using DAPI and GFP channels. The results were analysed and prepared in ZEN and Inkscape software.

4.2.2 Transfection of H1299 cell line

The H1299 cell line was chosen for transfection with a NPLOC4-GFP in pCMV6-AC-GFP vector containing Amp and Neo antibiotic resistance as selection markers. On day one 5 x 10^5 cells of the H1299 parental cell line were seeded in 2 ml of a complete medium in duplicate into a 6-well plate. After 24 hours of incubation, the transfection was done using Viromer® RED transfection reagents. In 300 µl of transfection buffer 2 µl of the plasmid DNA (concentration = 2 µg/µl) was added in a tube ´1´. Then 4 µl of Viromer® reagent was pipetted on a tube wall and 100 µl of transfection buffer was added in a tube ´2´. Reagents in tube ´2´ were mixed and vortexed. Reagents from tube ´1´ were added to tube ´2´, mixed and left for incubation for 15 min at RT. 200 µl of the reagents were added to each well. After 24 hours of incubation, the medium was removed and replaced with a fresh medium containing 1 mg/ml G 418 disulphate salt for an antibiotic selection.

After 24 hours of incubation, the cells were transferred into 25 cm^2 tissue culture flask with addition of medium containing G 418 at a concentration of 2.5 mg/ml. After three days of incubation, the cells were seeded into a 96-well plate. The prepared cell suspension contained 100 cells/10 ml and the volume per each well was 100 µl. The 96-well plate was placed in an incubator for two weeks until colonies grew from individual clones.

The cells were analysed for GFP signal using a confocal microscope. Four clones were selected, and the cells were transferred into 25 cm^2 tissue culture flasks. Western blot analysis was performed on all four clones.

4.2.3 Western blot

H1299 parental and H1299-NPL4-GFP cells were seeded into 22 cm^2 tissue culture dishes, concentration 5 x 10^5 cells in 4 ml of a complete medium. After 24 hours of incubation cell lysates were prepared. The medium was removed and 300 µl of 4X LSB

were added in the tissue culture dishes. The lysates were transferred into 1,5 ml tubes, vortexed and incubated for 5 min at 95 °C. Samples were loaded on 8% polyacrylamide gels and SDS-PAGE was performed.

Nitrocellulose membrane was washed with H_2O and 1X Transfer buffer. The gel and the membrane were both placed in a Semi-Dry Transfer Cell and the blotting was performed. The membrane was washed in TBS-Tween twice and once in H_2O. The membrane was placed in 5% milk in TBS-Tween for 60 min on a shaker. After the membrane was blocked, it was cut in half and prepared for primary antibody application. On one half of the membrane, the NPLOC4 Antibody (NBP1-82166) diluted 1:1 000 was added. On the other half of the membrane the β-Actin (C4), mouse monoclonal IgG antibody (sc-47778) diluted 1:500 was added. Both antibodies were diluted in 5% milk in TBS-Tween. Both membranes were incubated for one hour at RT.

The primary antibodies were removed, and the membrane was placed in TBS-Tween for 10 min on a shaker. Then Anti-Rabbit secondary antibody (NA934V) diluted 1:1 000 in was pipetted on the first half of the membrane and the Anti-Mouse secondary antibody (NA931V) diluted 1:1 000 was added on the second half of the membrane. Both antibodies were diluted in 5% milk in TBS-Tween. Incubation 45 min at RT. The secondary antibodies were removed, and the membranes were washed 3x5 min in TBS-Tween on a shaker. 300 µl per membrane of the chemiluminescent SuperSignal™ substrate were added and the measurement was performed using ChemiDoc Universal Hood III. The results were analysed in ImageLab software.

4.2.4 Flow cytometry assay

For flow cytometry analysis of the DTC-copper complexes a flow cytometry assay was developed. U2OS-NPL4-GFP and H1299-NPL4-GFP cell lines were used for the development. On day one 3 x 10^5 cells were seeded into 22 cm^2 tissue culture dishes with 4 ml of a complete medium. After 24 hours of incubation, cells were treated with 5 uM DTC-copper complexes. The same amount of DMSO at a final concentration 0.5% served as a control. After three hours of incubation, the medium was removed. On samples from both cell lines the pre-extraction was performed, however one sample from each cell line was not pre-extracted. These controls were prepared as follows: cells were washed with 1X PBS and 700 µl of Trypsine were added per tissue culture dish. Incubation for 10 min at 37 °C. 4 ml of a complete medium were added, mixed, and transferred into 15 ml

centrifuge tubes. Centrifugation 200 g, 3 min, RT. The supernatant was removed, the cells resuspended in 700 µl of 1X PBS, transferred into 1,5 ml tubes and put on ice. The measurement was performed.

The samples selected for pre-extraction were prepared as follows: cells were washed with 1X PBS and 700 µl of 1X PBS were added into the dish. The cells were scraped and transferred into 1,5 ml tubes and put on ice. Then 10% Triton was added to a final concentration of 0.1% and 10 µg/ml DAPI to a final concentration of 0.5 µg/ml. Incubation for 10 min on ice. The measurement was performed using BD Facs Verse. Measurements and results were analysed and prepared in BD FACSuite™, CytoSpec, Microsoft Excel 2016, Statistica 13 and Inkscape software.

4.2.5 Cytotoxicity assay

For measuring cytotoxicity, the XTT assay was performed. On day one 5 x 10^3 cells in 100 µl per well were seeded into a 96-well plate. Three wells were filled with 100 µl of a complete medium without cells as a blank. After 24 hours of incubation, the treatment was performed. The concentrations of DTC-copper complexes varied in different experiments, but two aspects were maintained in all cases. Firstly, the final concentration of DMSO was 0.5% in all wells including the control and secondly, the dilution between each DTC-copper complex concentration was two-fold, e.g., 25 nM, 50 nM, 100 nM etc.

After 48 hours of incubation 50 µl of XTT complete solution was added to all wells. Then the incubation time depended on the type of a cell line. The absorbance was measured at 475 nm and a reference measurement at 630 nm on a Plate reader, Infinite® 200 Pro. The results were analysed in Microsoft Excel 2016 software.

4.2.6 Isolation and purification of NPL4 protein

The bacterial culture of genetically modified *E. coli* BL21 (DE3) NPL4-GST (Novagen) was prepared. Bacteria were cultivated in an LB medium with ampicillin at a concentration of 100 µg/ml. Incubation at 37 °C, overnight, 180 rpm in a shaker/incubator. The bacterial culture was divided equally into Erlenmeyer flasks, where also LB medium was added, ampicillin at a concentration of 50 µg/ml and $ZnSO_4 \cdot 7H_2O$ at a concentration of 200 µM. The Erlenmeyer flasks were covered with aluminium foil, but not tightly. Incubation at 37 °C, three hours, 180 rpm in a shaker/incubator. All flasks

were transferred to a cooled incubator with a temperature set at 16 °C. Then 40 µl of 1 M IPTG were added to every flask. Incubation at 16 °C, overnight, 180 rpm in a shaker/incubator. SDS-PAGE of bacterial samples was performed before and after the addition of IPTG. Gels were stained with Coomassie Blue.

The content of Erlenmeyer flasks was taken out and transferred into 50 ml centrifuge tubes. Centrifugation 3 000 g, 5 min, RT. The supernatant was removed, and 4 ml of lysis buffer was added to the pellet. The lysis buffer contained PMSF at a concentration of 10 mM. The bacteria were resuspended and transferred into 2 ml tubes. The tubes were placed on ice and lysis was performed using an ultrasonic homogenizer. Centrifugation 15 000 g, 2 min at 4 °C. The supernatant was transferred into 15 ml centrifuge tubes and loaded on 8% polyacrylamide gels. SDS-PAGE was performed with Coomassie Blue staining.

Samples were loaded on the FPLC-NGC Chromatography System with a GST cartridge installed. Elution was performed using the elution buffer containing 20 mM glutathione, fractions were collected and kept on ice. The GST fractions were loaded on 8% polyacrylamide gels and SDS-PAGE was performed with Coomassie Blue staining. The GST fractions were loaded on the FPLC-NGC Chromatography System with two desalting columns installed. Elution was performed using the phosphate buffer, fractions were collected and kept on ice. The fractions were loaded on 8% polyacrylamide gels and SDS-PAGE was performed with Coomassie Blue staining. All FPLC measurements and analyses were performed in ChromLab software.

The final step of the purification process was the concentration of NPL4 protein. Centrifugal filters and microtubes with 30K membrane were used. After loading 400 µl of the fraction the centrifugation was performed at 4 °C, 15 000 g, 5 min. The supernatant was removed and loading and the centrifugation process was repeated until the final volume of the concentrated and purified protein was 400 µl. Bradford assay was performed to determine protein concentration.

4.2.7 Drug Affinity Responsive Target Stability (DARTS)

Purified NPL4 protein was diluted by a phosphate buffer, pH 7.4 to a final concentration of 0.03 µg/µl. The protein was treated with 10 µM DTC-copper complexes, incubated for one hour at RT. An equal amount of DMSO added to the diluted protein served as a control sample. Pronase dissolved in the TNC buffer was added to the samples

to a final concentration of 0.75 µg/ml, incubation for 90 min at 37 °C. A sample without Pronase served as a control. The reaction was stopped with 4X LSB and the samples were incubated for 5 min at 95 °C. The samples were loaded on 10%, 1,5 mm polyacrylamide gels and SDS-PAGE was performed with an electrophoretic cell placed on ice. The gels were stained with a SilverQuest^{TM} staining kit.

4.2.8 Synthesis of DTC-copper complexes

The synthesis was done as previously described in ref[78]. Briefly, in 15 ml centrifuge tube, 10 ml of distilled water was added. Then 1 ml of 100 mM $CuCl_2$ was added. After a short vortex, 2 ml of 100 mM DTC dissolved in water were added and mixed. Centrifugation at RT, 1 000 g, 5 min. The supernatant was removed, and 10 ml of purified water was added and mixed. This step with the centrifugation was repeated two times. The supernatant was removed, and the centrifuge tubes were placed into a vacuum desiccator without caps, until the pellets were dried.

4.2.9 Statistical analyses

Pearson´s correlation was performed to evaluate flow cytometry and cytotoxicity screenings of DTC-copper complexes using the software Statistica 13. For other experiments, statistics such as error bars, number of repetitions, etc. are specified in figure legends.

5 RESULTS

5.1 CuET Induces NPL4 Aggregation

The effect of CuET on the p97 cofactor NPL4 in cancer cells has already been observed and published. CuET causes NPL4 aggregates that trigger heat shock response and results in cell death[69]. To confirm these results an experiment was performed on U2OS-NPL4-GFP cell line. After 1 μM CuET treatment for three hours the cells were fixated and NPL4 aggregates were observed in the cytoplasm (**Fig. 6A**) using confocal microscopy. A change in the pattern of NPL4 occurred compared to mock. Next, a pre-extracion was performed to see whether the aggregates are insoluble. As a result soluble proteins were removed from the cells and no GFP signal was detected in mock. However, in CuET treated cells the NPL4 aggregates were present in the cytoplasm (**Fig. 6B**). The results confirmed the published data and verified the phenotype of U2OS-NPL4-GFP cell line.

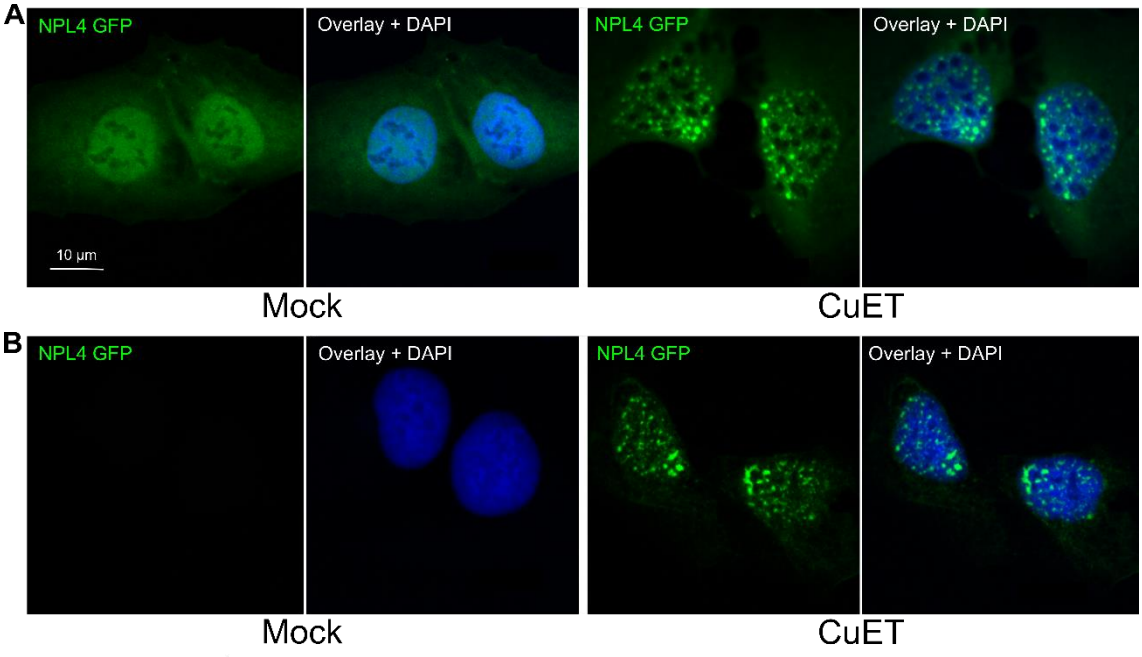

Figure 6: NPL4 aggregates in U2OS-NPL4-GFP cells after CuET treatment. (**A**) CuET immobilizes NPL4 in the cytoplasm. Cells were treated with 1 μM CuET for three hours and fixated. (**B**) NPL4 aggregates are present in the cells after 1 μM CuET three-hour treatment and pre-extraction. Data are representative of two independent experiments.

5.2 Development of H1299-NPL4-GFP Cell Line

Next, I wanted to know whether the CuET effect on NPL4 occurs in U2OS cells only or in another cancer cell line as well. For that purpose H1299 cell line was selected and transfected with NPLOC4-GFP in pCMV6-AC-GFP vector. The transfection was successful and four H1299-NPL4-GFP clones were developed and selected. Western blot was performed to confirm NPL4-GFP expression in the developed clones. The results showed that only clones 2 and 3 expressed NPL4-GFP (**Fig. 7**). Both clones 2 and 3 were then tested for NPL4-GFP expression using flow cytometry and as a result clone 2 was selected for further analyses due to its uniform population (data not shown).

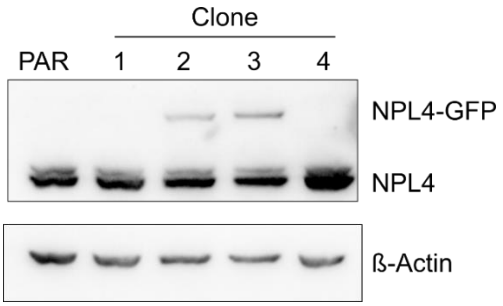

Figure 7: Western blot of four transfected H1299-NPL4-GFP clones. Clones 2 and 3 expressed NPL4-GFP. Clone 2 was selected for further experiments because of its uniform population. Parental cell line (PAR) served as a control.

5.3 Screening of DTCs as Potential NPL4 Inhibitors Using a Developed Assay

5.3.1 Development of an Assay

The observed CuET effect on NPL4 was an interesting result of its mechanism in cancer cells. NPL4 remained immobilized in the cytoplasm after pre-extraction. This fact was the motive for the development of an assay that could be used to screen other similar substances with a possible antitumour effect. The question was whether copper complexes of other DTCs have the same effect on NPL4 as CuET? CuET is a copper complex that is formed in the body after the administration of DSF. DSF belongs to the group of DTCs. So the assay will be suitable for the screening of DTC-copper complexes and their effect on NPL4.

U2OS-NPL4-GFP and transfected H1299-NPL4-GFP cell lines were used in the assay development. At first it was necessary to confirm that no signal of NPL4-GFP is

present in cells after pre-extraction. Fluorescence of NPL4-GFP in cells was measured before and after pre-extraction. A significant decrease in fluorescence was observed after pre-extraction (**Fig. 8A**) because all soluble proteins including NPL4 were removed from the cells. Subsequently cells were treated with 5 µM CuET and after three-hour incubation pre-extracted. High fluorescence after CuET treatment confirmed the data from microscopy. CuET immobilizes NPL4 in the cells and therefore fluorescence is detected after pre-extracion (**Fig. 8B**). The assay was successfully developed and was suitable for the screening.

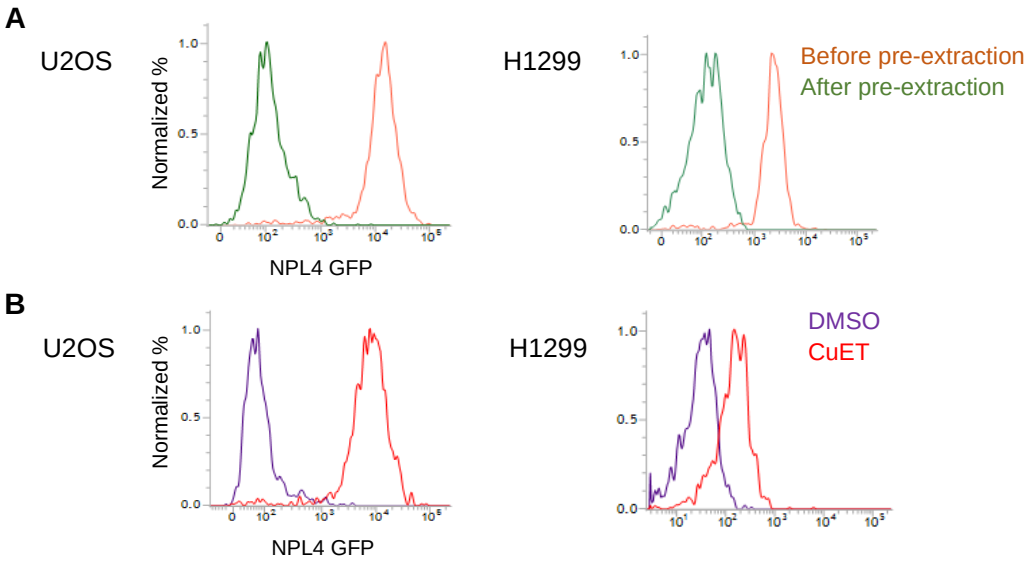

Figure 8: Flow cytometry assay. (**A**) Decrease of fluorescence after pre-extraction. Soluble proteins including NPL4-GFP are removed from the cells. (**B**) Fluorescence of immobilized NPL4-GFP detected after 5 µM CuET three-hour treatment in pre-extracted cells. Data are representative of three independent experiments.

5.3.2 DTC-copper Complexes Differ in the Effect on NPL4

All twelve DTCs were tested for their effect on NPL4 using the developed flow cytometry assay. The screening was performed on U2OS-NPL4-GFP cell line. DTCs were mixed with $CuCl_2$ in a ratio of 2:1 in DMSO to form DTC-copper complexes. Then the cells were treated with 5 µM concentration for three hours and pre-extracted. The fluorescence of immobilized NPL4-GFP after pre-extraction was detected in six compounds – CuET, 1, 2, 7, 9, and 11 (**Fig. 9**). Due to their positive effect on NPL4 these six compounds were chosen for further experiments and were also tested on H1299-NPL4-GFP cell line. The effect on NPL4 of these compounds was confirmed on this cell

line except for compound 9 (**Fig. 10**). The result of the screening showed that some of the copper complexes of other DTCs have the same effect on NPL4 as CuET.

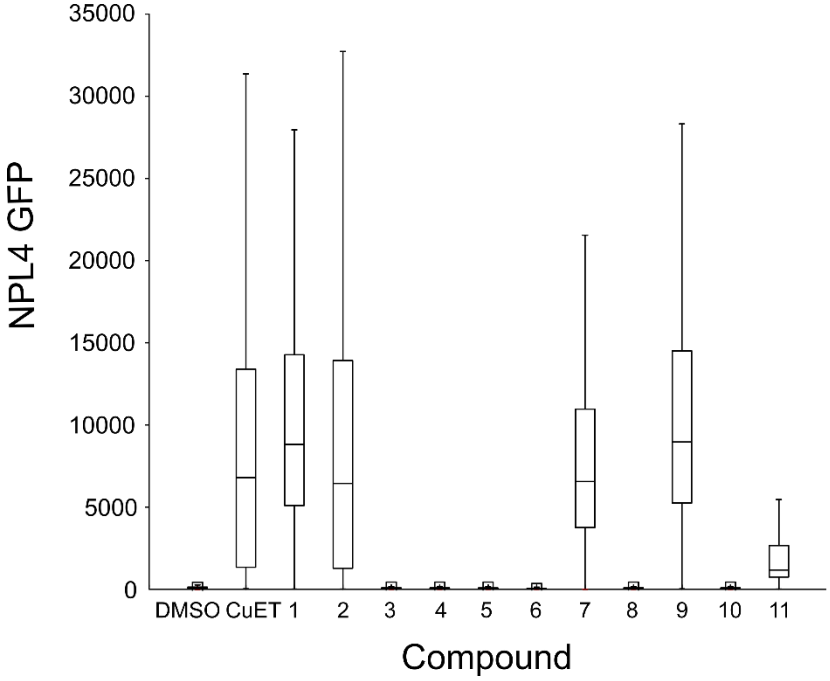

Figure 9: Flow cytometry screening of DTC-copper complexes effect on NPL4 on U2OS-NPL4-GFP cell line. Concentration of all compounds was 5 μM, three-hour incubation. Box plots show median, 25%-75% and non-outlier range. Data are representative of two independent experiments.

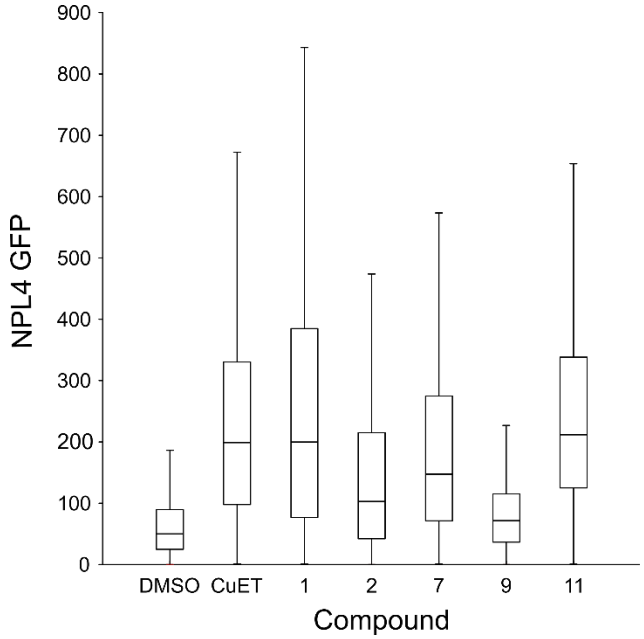

Figure 10: Flow cytometry screening of active DTC-copper complexes on H1299-NPL4-GFP cell line. Concentration of all compounds was 5 μM, three-hour incubation. Box plots show median, 25%-75% and non-outlier range. Data are representative of two independent experiments.

5.3.3 Testing of Additional Concentrations of Active Compounds

The compounds with a positive NPL4 effect from the screening were tested at lower concentrations on U2OS-NPL4-GFP cells. The purpose was to find out at what concentration NPL4 effect still occurs and whether this effect is concentration dependent. U2OS-NPL4-GFP cells were treated with 5 µM, 1 µM, 0.5 µM and 0.1 µM concentrations of the active compounds – CuET, 1, 2, 7, 9, 11 – for three hours and pre-extracted. Compounds CuET, 1, 2, 7 were effective even at a lower concentration of 0.5 µM, while compounds 9 and 11 did not show sufficient activity at lower concentrations. None of the substances was active at the lowest concentration of 0.1 µM (**Fig. 11**). Experiments were performed on U2OS-NPL4-GFP cell line only due to low NPL4-GFP intensity in H1299. The result showed that the effect on NPL4 increased in a concentration dependent manner and that some compounds showed NPL4 effect even at a concentration of 0.5 µM.

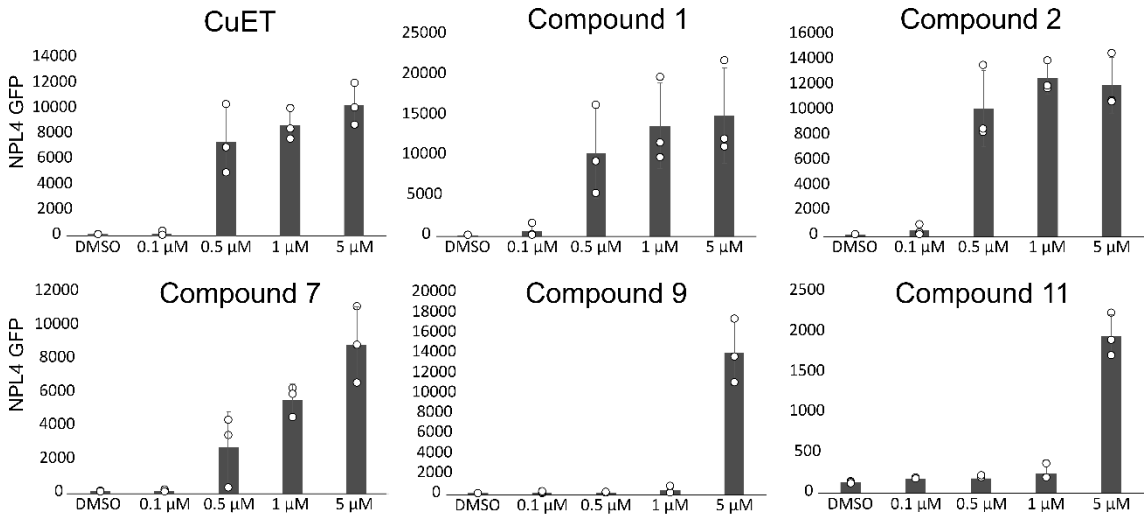

Figure 11: Flow cytometry analyses of additional concentrations of active compounds. U2OS-NPL4-GFP cells were treated with 5 µM, 1 µM, 0.5 µM and 0.1 µM DTC-copper complexes for three hours and pre-extracted. Data are mean ± s.d. of three independent experiments.

5.4 Different Cytotoxicity of DTC-copper Complexes

However, the effect on NPL4 of the compounds alone did not in itself provide any information on viability of the cancer cells. Therefore another step in the screening of DTCs was the measurement of cytotoxicity. XTT assay was performed with all DTC-copper complexes on both U2OS and H1299 cell lines. Cells were treated with 5 µM concentration for 48 hours. Experiments were performed in triplicates and repeated two times. The results showed that cytotoxicity is associated with the effect on NPL4 of the compounds except for compound 8 (**Fig. 12**).

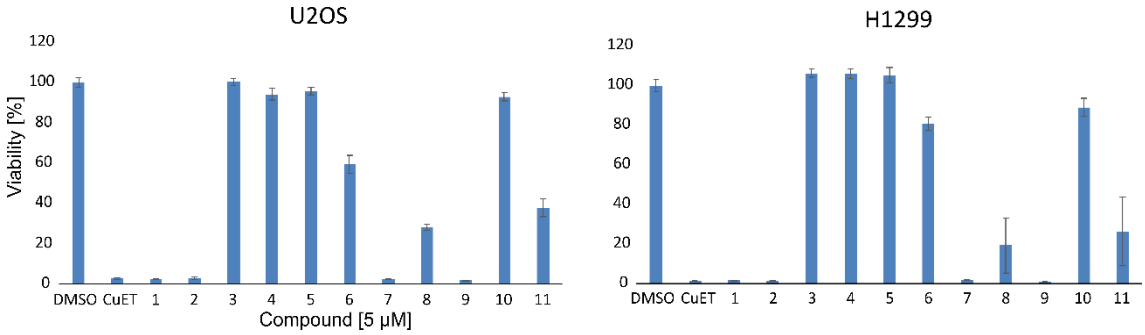

Figure 12: Cytotoxicity analysis of DTC-copper complexes. Both cell lines were treated with 5 µM concentration for 48 hours. Data are representative of two independent experiments. Bars display mean ± s.d. from triplicates.

5.5 The Effect on NPL4 Correlates Positively with Cytotoxicity

The flow cytometric screening showed that certain DTC-copper complexes, including CuET, caused NPL4 aggregation. The cytotoxicity results showed that compounds that decreased the viability of cancer cells were the same that had the effect on NPL4. So the data were evaluated by Pearson´s correlation and a positive correlation between the effect on NPL4 and cytotoxicity was found in DTC-copper complexes (R^2 = 0.6865, p = 0.0009) (**Fig. 13**). Therefore the effect on NPL4 of DTC-copper complexes is associated with cell viability in cancer cells. However, compound 8 did not follow this scheme. The compound was cytotoxic but did not cause NPL4 aggregation on flow cytometry (**Fig. 9**). This suggests that the mechanism of the substance is different from NPL4 immobilization.

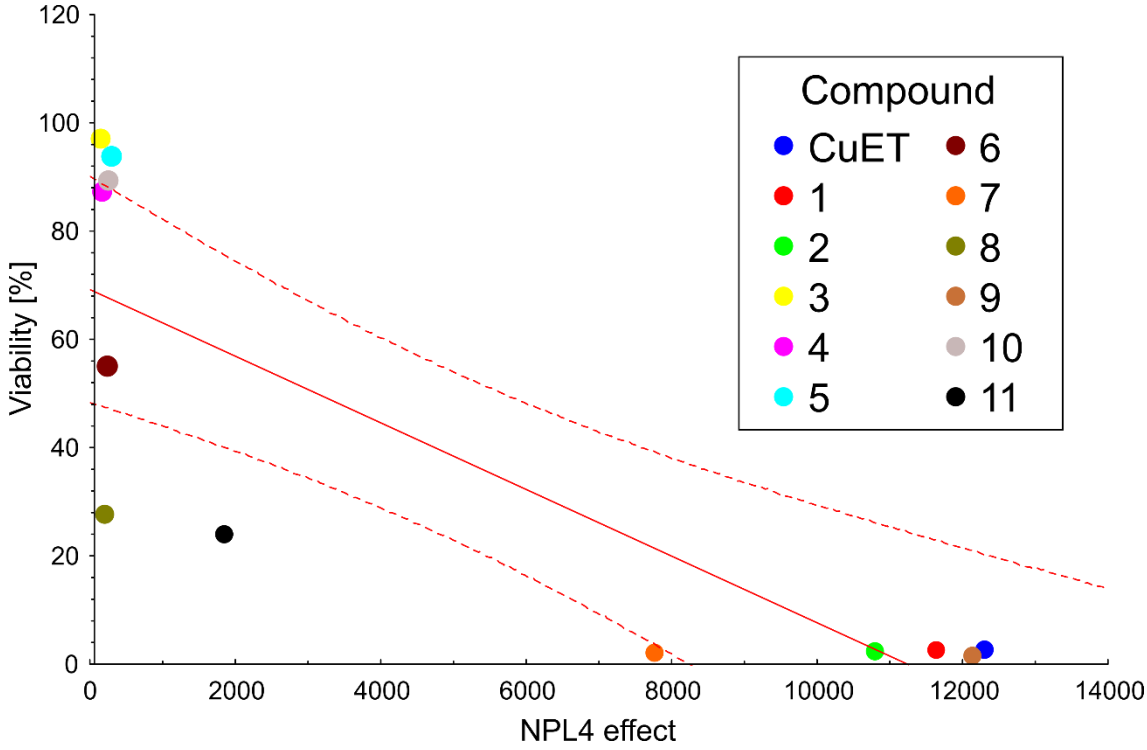

Figure 13: Correlation between the effect on NPL4 and cytotoxicity in DTC-copper complexes. A positive correlation was found (R^2 = 0.6865, p = 0.0009). Except for compound 8 which decreased cell viability in cytotoxicity assays, but no NPL4 effect was observed in flow cytometry. Dashed lines represent the 95% confidence interval.

5.6 Isolation and Purification of NPL4 for *in vitro* Assay

Correlation between the effect on NPL4 and cytotoxicity was observed in cell experiments. Nevertheless, there are thousands of proteins, molecules and biochemical reactions that happen inside of the cell. Therefore a biochemical *in vitro* assay was prepared to determine if the DTC-copper interaction would occur on the purified protein. So it was necessary to obtain a purified NPL4 protein. For that purpose, genetically modified *E. coli* BL21 (DE3) NPL4-GST (Novagen) was used. This bacterial cell line was created and described in[69].

During bacterial cultivation, the IPTG was added to induce the expression of the desired NPL4. The bacterial samples were acquired before and after the IPTG addition and SDS-PAGE was performed to see whether NPL4-GST expression was induced. Bands with high intensity of ~90 kDa after Coomassie staining confirmed the expression (**Fig. 14A**). The next step was bacterial lysis after incubation. The bacterial cells were lysed on ice by an ultrasonic homogenizer and SDS-PAGE was performed on bacterial

lysates. The whole bacterial proteome could be seen on the gel, including the band of NPL4-GST with the highest intensity (**Fig. 14B**).

Samples from bacterial lysis were purified using FPLC. GST cartridges were used for affinity purification and SDS-PAGE was performed on collected fractions. Bands of NPL4-GST without bacterial proteins were visible on the gel (**Fig. 15A**). Then desalting columns were used to remove small molecules and then SDS-PAGE was performed on the collected diluted (**Fig. 15B**) and concentrated fractions (**Fig. 15C**). The final step was the concentration of the purified NPL4 protein and Bradford assay to determine its concentration. NPL4 protein was successfully isolated and purified from the bacterial cells and ready for biochemical *in vitro* experiments.

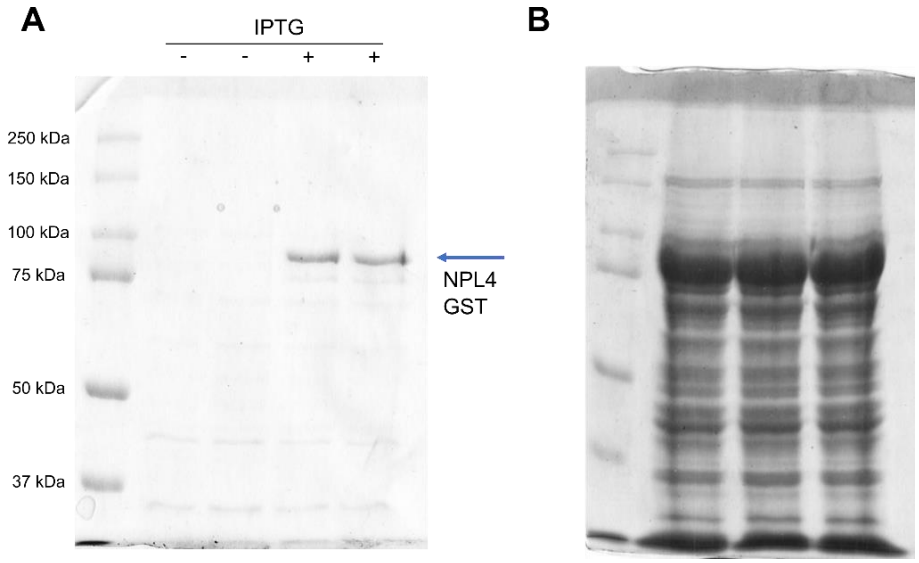

Figure 14: SDS-PAGE results from NPL4-GST isolation from *E. coli*. (**A**) Samples were taken before and after IPTG addition. (**B**) A whole bacterial proteome, including the band of NPL4-GST with the highest intensity after bacterial lysis.

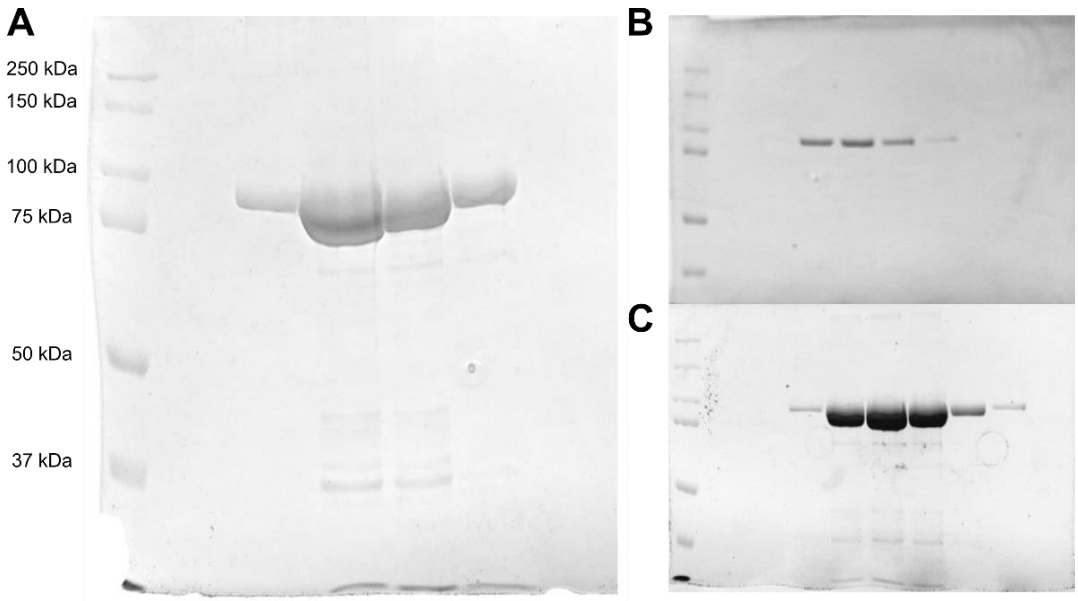

Figure 15: SDS-PAGE results from FPLC purification. (**A**) Collected fractions from the affinity purification by GST cartridges. NPL4-GST bands without bacterial proteins. (**B**) Collected diluted and (**C**) concentrated fractions from the desalting columns.

5.7 DTC-Copper Causes NPL4 Conformational Change *in vitro*

In order to see NPL4-DTC-copper interaction *in vitro* the purified NPL4 protein was used. The DARTS method that uses the proteolytic enzyme Pronase was used in the experiment. The purified NPL4 protein was incubated with Pronase resulting in the formation of smaller fragments. In the presence of a NPL4-interacting compound, the cleavage pattern was changed most likely due to a conformational change of NPL4. The method was optimized (**Fig. 16A**), and western blot was performed with monoclonal and polyclonal NPL4 antibodies. The result showed that more differentiated bands were seen after using the polyclonal antibody (**Fig. 16B**).

Another DARTS experiment was performed to find out how the interactions for other DTC-copper complexes would look like. The complexes of compounds CuET, 1, 2 and 3 were synthesized and used for the treatment of the purified NPL4. The second DARTS experiment confirmed the flow cytometry results. Active compounds interacted with NPL4 and showed a different cleavage pattern in the presence of Pronase (**Fig. 17**). Compound 3 which had no effect on NPL4 on flow cytometry (**Fig. 9**) did not interact with NPL4 on DARTS.

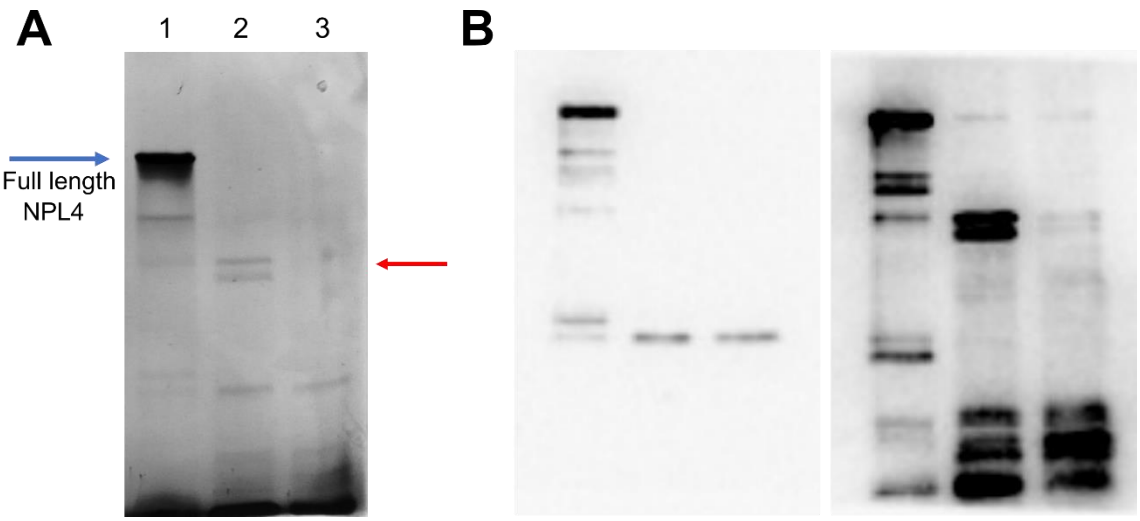

Figure 16: DARTS optimization. (**A**) A change of cleavage pattern in the presence of NPL4 interacting compound (**red arrow**). 1 – Control; 2 – Pronase 0.75 µg/ml; 3 – Treatment with 10 µM CuET. Samples were incubated for 60 minutes at RT with CuET. Incubation with Pronase at 37 °C for 90 minutes. (**B**) Western blot of DARTS results. **Left:** Monoclonal NPL4 antibody. **Right:** Polyclonal NPL4 antibody.

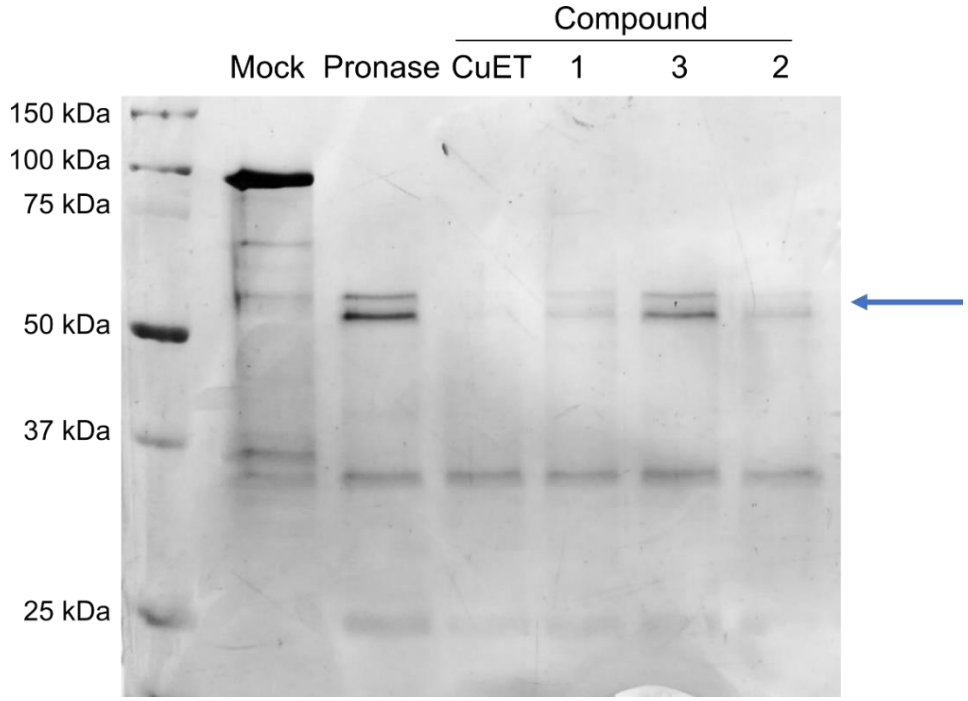

Figure 17: DARTS results. DTC-copper complexes CuET, 1, 2, 3 were synthesized and used in the experiment. Active compounds CuET, 1, 2 interacted with the purified NPL4 and after proteolysis by Pronase the cleavage pattern was changed (**arrow**).

5.8 Synergy of CuET and Copper

An interesting phenomenon has been observed during experiments and analyses. CuET as a cytotoxic compound itself, which already contains a copper(II) atom, showed synergy with the added copper in the form of $CuCl_2$ that resulted in even higher cytotoxicity in cancer cells. Cytotoxicity of $CuCl_2$ alone was ruled out by a cytotoxicity assay, when very high concentrations resulted in a decrease in viability (**Fig. 18A, B**). While in combination with CuET a cytotoxic effect was observed after the addition of 5 µM $CuCl_2$. This experiment was performed on both U2OS and H199 cell lines with the same result.

Next experiment was to test whether the effect is a feature of CuET only or whether it also occurs in other DTC-copper complexes. Also, if the synergy is able to increase the toxicity of the compound which was not cytotoxic in itself. Compounds 1, 2, and 3 were tested for synergy and were added to the U2OS cells after 10 µM $CuCl_2$ treatment. Synergy was observed in compounds 1 and 2 (**Fig. 19A, B**) but no effect was observed in compound 3 (**Fig. 19C**). This result confirmed the synergistic effect in other compounds and also showed that synergy does not affect a non-cytotoxic compound, its activity remains the same.

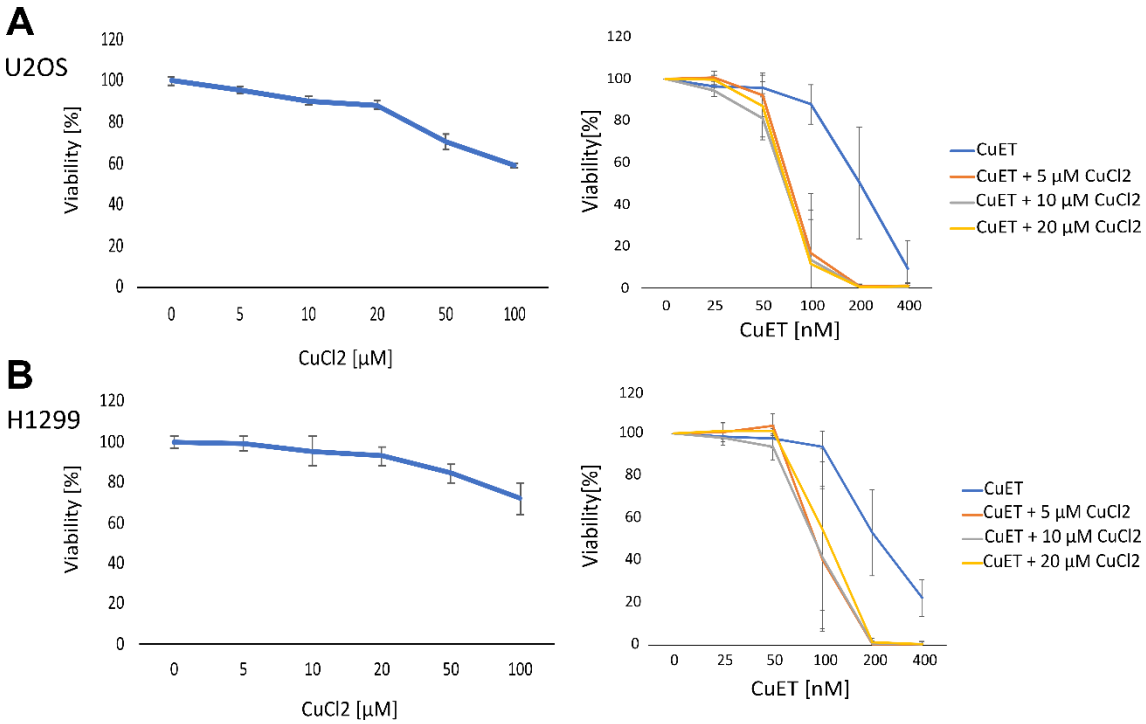

Figure 18: Synergy of CuET and copper. In (**A**) U2OS and (**B**) H1299 cells no toxicity of copper was observed until the cells were treated with very high concentrations. After the addition of CuET the cytotoxic concentrations significantly decreased. Data represent mean ± s.d. from three independent experiments.

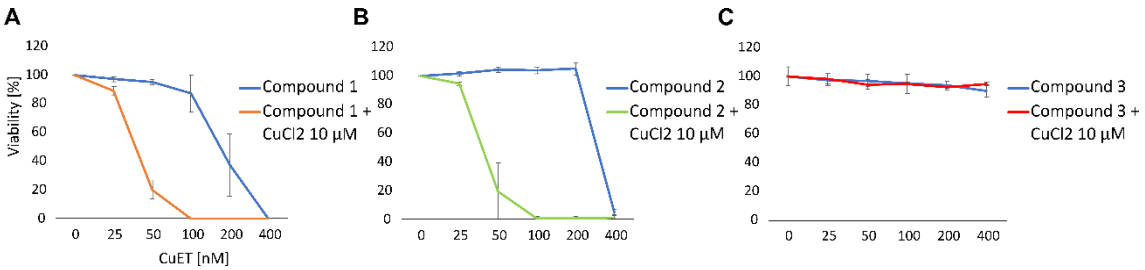

Figure 19: Synergy of other DTC-copper complexes with copper. After 10 µM $CuCl_2$ treatment U2OS cells were treated with various concentrations of (**A**) compound 1, (**B**) compound 2 and (**C**) Compound 3. Compouond 3 did not show any synergistic effect. Data represent mean ± s.d. from three independent experiments.

When the copper synergy with other DTC-copper complexes was confirmed, we wanted to know whether other metals will have the same effect. U2OS cells were treated with 10 µM solutions containing either zinc, cadmium or iron(III) and then CuET in various concentrations was added. No synergy was observed except for the cadmium (**Fig. 20**).

Finally, we decided to test whether the principle of synergy is associated with NPL4 or not. If cytotoxic effects are increased, will it affect NPL4 in any way? Will the effect on NPL4 also increase or remain the same? The developed flow cytometry assay was used for answering these questions. The mechanism with NPL4 involvement was confirmed. A lower concentration of CuET in combination with 10 µM $CuCl_2$ was needed for the effect on NPL4 compared to previous experiments (**Fig. 21**). NPL4 appears to be the key player responsible for the CuET-copper synergy.

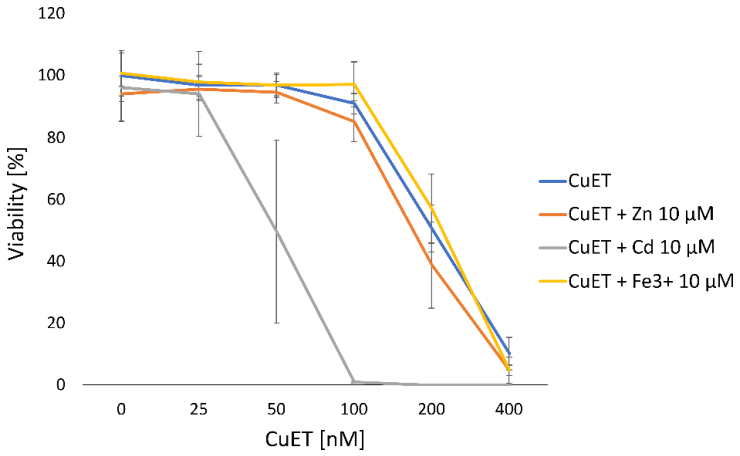

Figure 20: Synergy between CuET and other metals. Synergy was observed only for cadmium of all tested metals. Data represent mean ± s.d. from three independent experiments.

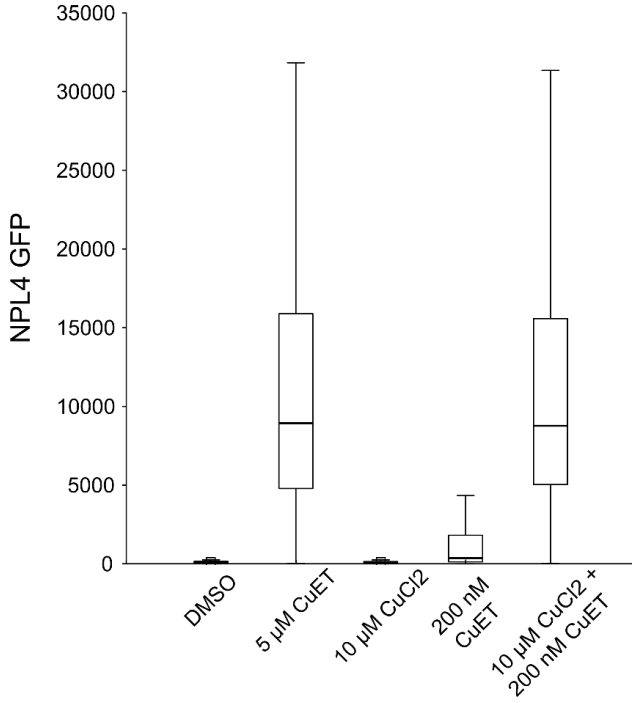

Figure 21: Flow cytometry assay confirms the involvement of NPL4 in CuET-copper synergy. Box plots show median, 25%-75% and non-outlier range. Data are representative of three independent experiments.

6 DISCUSSION

In this thesis, I focused on the identification of new possible NPL4 inhibitors and their mechanism of action. All of the tested compounds belonged to the group of DTCs. The results bring promising prospects for the use of DTCs as potential new anticancer therapeutics. DSF and its metabolite CuET have already come to the forefront of interest due to their antitumour abilities[79].

The results confirmed the published data[69] when CuET caused aggregates of NPL4 that were observed using confocal microscopy. Since DTCs react easily with metals, DTC-copper complexes were prepared and tested for their effect on NPL4 using the developed flow cytometry assay. Six of twelve complexes had an effect on NPL4 in cancer cells and showed antitumour activity. The inhibition of NPL4 was shown to compromise the whole p97 pathway resulting in inhibition of protein degradation, triggering a heat shock response and cell death[69]. These findings point to NPL4 as an excellent target for anticancer therapy. In addition, the fact that higher expression of NPL4 was reported in certain types of cancer[49,50] and is also associated with poor prognosis speaks in favour of this. Several publications already focused on NPL4 as the target in medulloblastoma[80], renal cell carcinoma[49] and multiple myeloma[72]. Another positive, but no less significant, is that the development of CuET resistance in cancer cells has not yet been reported.

The DARTS method that was performed to confirm NPL4-DTC-copper interaction *in vitro* was initially developed to identify protein interactions with small molecules. The strategy was to stabilize the target proteins by drug binding. A small drug molecule binds to a protein and thereby stabilizes its conformation during proteolysis. The cleavage pattern is changed and can be seen on the gel after silver staining. The stabilized protein with bound molecule represent bands of higher intensity in contrast to the cleaved control[81]. The method has already been used to observe the interaction between CuET and NPL4 *in vitro*[69]. I successfully reproduced these results and used the method to see NPL4 interaction with other DTC-copper complexes. The data from my DARTS experiments showed that after the purified NPL4 was incubated with CuET, the cleavage pattern changed. A change in NPL4 conformation occurred which appeared on the gel as a band with weaker intensity. The DARTS method was used for a different purpose than in the original publication and the results also differ, but showed that

a conformational change in NPL4 occurs due to the interaction with CuET and other active DTC-copper complexes.

The evaluation of DTC-copper complexes screening revealed a positive correlation between the effect on NPL4 and cytotoxicity. All six compounds that caused NPL4 immobilization also decreased the viability of cancer cells in two cell lines. That means that NPL4 is likely the key target of the anticancer mechanism of CuET and other DTC-copper complexes. The exception was compound 8 which reduced the viability but had no effect on NPL4, suggesting a different target of its antitumour mechanism other than NPL4. The DARTS results showed that compounds that had the effect on NPL4 and were cytotoxic also interacted with purified NPL4 *in vitro*. Compound 3 which had no effect on NPL4 nor was cytotoxic did not interact with NPL4 on DARTS. Probably for steric reasons, because it is a larger molecule in comparison to active compounds such as CuET, compound 1 and 2.

During the experiments, a synergy between copper and CuET was found that increased the anticancer effect of CuET for its lower concentrations. Subsequently, the synergy was confirmed for other tested DTC-copper complexes. This experiment also confirmed that the addition of extra copper did not increase the potency of otherwise non-toxic compounds, such as compound 3. Of other metals, synergy has also been observed in CuET and cadmium. Cadmium is a toxic substance in itself[82] and this is probably why it enhances the effect of CuET. The involvement of NPL4 in the mechanism of synergy was confirmed using the developed flow cytometry assay. CuET at high concentrations immobilized NPL4 in the cytoplasm and high fluorescence of NPL4-GFP was detected. Synergy with CuET occurred after copper addition and the same effect on NPL4 was observed even at lower CuET concentration which itself had only a minor effect on NPL4 immobilization.

A phenomenon of synergy has already been observed in anticancer therapy[83]. However, this is a very complex matter and many factors need to be considered, including the concentration, dosage and contraindications of individual chemotherapeutics. Due to such complexity, machine learning techniques are used to predict possible combinations[84]. In contrast, the synergy observed between CuET and copper seems simple, but its result significantly increases the antitumour effect.

An interesting insight into NPL4 structure using cryo-electron microscopy was published recently[85]. According to the published data NPL4 binds to the N domain of p97 with one zinc finger motif. The same publication suggested a mechanism of p97 inhibition

by CuET. After CuET treatment, free copper ions were released under oxidative conditions. These copper ions inhibited the unfolding activity of p97. Authors claim that CuET serves only as an ionophore and the copper ions themselves interact with zinc finger domains of NPL4, lock its conformation and therefore inhibit p97. This mechanism is said to occur only in cancer cells where ROS induce the release of copper ions from CuET[85]. Nevertheless, this statement does not consider the fact that there is already an excess of copper in cancer cells and the described mechanism would occur spontaneously without the aid of CuET. In addition, my DARTS experiments confirmed the interaction between NPL4 and CuET *in vitro*.

Certain publications suggest that DSF and CuET are proteasome inhibitors[66,71]. However, the results from my thesis indicate the inhibition of the upstream segment in p97 pathway which is NPL4. The possible explanation regarding the proteasome inhibition could be that when copper(I) or (II) is used alone it has a potential to inhibit 20S proteasome and induce cell death[86]. However, when copper is used in DTC-copper complex the target is NPL4 as confirmed by other studies[69,70].

In a recent publication, Tsvetkov *et al.* showed a different kind of mechanism how copper ionophores induce cell death[87]. Authors suggest that cuproptosis – a type of cell death accompanied by a large amount of copper accumulation – occurs by direct binding of copper to lipoylated proteins that results in toxic protein aggregation, proteotoxic stress and cell death. None of the results included NPL4 inhibition or the p97 pathway. The lipoylated proteins are part of the Krebs cycle. In other words, the phenotype of the cells was associated with mitochondrial respiration and not glycolytic one. However, the authors mentioned that cells were cultivated under glycolytic conditions. Also, no explanation has been provided for the link between the aggregated proteins and cell death.

Factors including low price, anticancer activity and easy availability support the idea of the use of DSF and other DTCs as effective chemotherapeutics against cancer both in developed and developing countries. Cancer treatments in the vast majority mean a financial burden for the health system and the patients themselves. For example, average costs of medical care and oral prescription drugs for patients with cancer in the USA in 2015 were $183 billion with a prognosis based on population growth to increase to $246 billion by 2030.[88] In addition, the cost of development of new anticancer drugs with an unknown efficacy in clinical trials range in the millions of dollars[89]. Non-profit drugs such as DSF might be a solution to this problem, because generic drugs are affordable and well known for decades. The only obstacle is the funding of clinical trials

which can be addressed through the involvement of governments and charities[90]. One of the examples could be the Bill & Melinda Gates Foundation which donated $15.1 million to an international consortium of researchers to develop new drugs against sleeping sickness and leishmaniasis[91]. However, DSF is already a developed drug and its clinical use would facilitate the fight against cancer financially, but above all it would help countless patients.

7 CONCLUSION AND FUTURE PERSPECTIVES

Aims of the thesis were successfully accomplished. A flow cytometry assay was developed for the screening of DTC-copper complexes effect on NPL4. Six of twelve tested complexes immobilized NPL4 in the cancer cells. The cytotoxicity screening was performed and a positive correlation was found between the cytotoxicity and effect on NPL4. Except for compound 8 which showed positive results in cytotoxicity but had no effect on NPL4. The interaction between DTC-copper complexes and NPL4 was confirmed using *in vitro* DARTS reaction. New NPL4 inhibitors were successfully characterized. In addition, a synergy of DTC-copper complexes and copper has been found that increased the cytotoxicity of complexes in cancer cells. The mechanism of the synergy was confirmed to be associated with NPL4.

In the future, it is planned to do the screening of new DTC-copper complexes, that will be provided by the collaborating laboratory, and test their effect on NPL4. Certainly, new experiments will be planned regarding the mechanism of synergy. Such an interesting phenomenon needs to be explained and might push the potential of DTCs as possible future anticancer therapeutics even further.

8 REFERENCES

1. Hartl, F. U. Protein misfolding diseases. *Annu. Rev. Biochem.* **86**, 21–26 (2017).

2. Chiti, F. & Dobson, C. M. Protein Misfolding, Functional Amyloid, and Human Disease. *Annu. Rev. Biochem.* **75**, 333–366 (2006).

3. Hipp, M. S., Park, S. H. & Hartl, U. U. Proteostasis impairment in protein-misfolding and -aggregation diseases. *Trends Cell Biol.* **24**, 506–514 (2014).

4. Kim, Y. E., Hipp, M. S., Bracher, A., Hayer-Hartl, M. & Ulrich Hartl, F. Molecular chaperone functions in protein folding and proteostasis. *Annual Review of Biochemistry* **82**, 323–355 (2013).

5. Gomez-Pastor, R., Burchfiel, E. T. & Thiele, D. J. Regulation of heat shock transcription factors and their roles in physiology and disease. *Nat. Rev. Mol. Cell Biol. 2017* **19**, 4–19 (2017).

6. Richter, K., Haslbeck, M. & Buchner, J. The Heat Shock Response: Life on the Verge of Death. *Mol. Cell* **40**, 253–266 (2010).

7. David, D. C. *et al.* Widespread Protein Aggregation as an Inherent Part of Aging in C. elegans. *PLOS Biol.* **8**, e1000450 (2010).

8. Hanahan, D. & Weinberg, R. A. Hallmarks of cancer: The next generation. *Cell* **144**, 646–674 (2011).

9. Ben-David, U. & Amon, A. Context is everything: aneuploidy in cancer. *Nat. Rev. Genet. 2019 211* **21**, 44–62 (2019).

10. Bielski, C. M. *et al.* Genome doubling shapes the evolution and prognosis of advanced cancers. *Nat. Genet.* **50**, 1189 (2018).

11. Brancolini, C. & Iuliano, L. Proteotoxic Stress and Cell Death in Cancer Cells. *Cancers (Basel).* **12**, 1–22 (2020).

12. Deshaies, R. J. Proteotoxic crisis, the ubiquitin-proteasome system, and cancer therapy. *BMC Medicine* **12**, (2014).

13. Santarosa, M., Favaro, D., Quaia, M. & Galligioni, E. Expression of heat shock protein 72 in renal cell carcinoma: Possible role and prognostic implications in cancer patients. *Eur. J. Cancer* **33**, 873–877 (1997).

14. Mitsiades, C. S. *et al.* Antimyeloma activity of heat shock protein-90 inhibition. *Blood* **107**, 1092–1100 (2006).

15. Khong, T. & Spencer, A. Targeting HSP 90 induces apoptosis and inhibits critical survival and proliferation pathways in multiple myeloma. *Mol. Cancer Ther.* **10**, 1909–1917 (2011).

16. Mendillo, M. L. *et al.* HSF1 drives a transcriptional program distinct from heat shock to support highly malignant human cancers. *Cell* **150**, 549 (2012).

17. Dai, C. & Sampson, S. B. HSF1: Guardian of Proteostasis in Cancer. *Trends Cell Biol.* **26**, 17–28 (2016).

18. Finley, D. Recognition and processing of ubiquitin-protein conjugates by the proteasome. *Annual Review of Biochemistry* **78**, 477–513 (2009).

19. Majumder, P. & Baumeister, W. Proteasomes: Unfoldase-assisted protein degradation machines. *Biol. Chem.* **401**, 183–199 (2019).

20. Hideshima, T. *et al.* Small-molecule inhibition of proteasome and aggresome function induces synergistic antitumor activity in multiple myeloma. *Proc. Natl. Acad. Sci. U. S. A.* **102**, 8567–8572 (2005).

21. Goy, A. *et al.* Phase II study of proteasome inhibitor bortezomib in relapsed or refractory B-cell non-Hodgkin's lymphoma. *J. Clin. Oncol.* **23**, 667–675 (2005).

22. Manasanch, E. E. & Orlowski, R. Z. Proteasome Inhibitors in Cancer Therapy. *Nat. Rev. Clin. Oncol.* **14**, 417 (2017).

23. Huang, Z. *et al.* Efficacy of therapy with bortezomib in solid tumors: a review based on 32 clinical trials. *Futur. Oncol.* **10**, 1795–1807 (2014).

24. Lü, S. *et al.* Point Mutation of the Proteasome β5 Subunit Gene Is an Important Mechanism of Bortezomib Resistance in Bortezomib-Selected Variants of Jurkat T Cell Lymphoblastic Lymphoma/Leukemia Line. *J. Pharmacol. Exp. Ther.* **326**, 423–431 (2008).

25. Oerlemans, R. *et al.* Molecular basis of bortezomib resistance: proteasome subunit β5 (PSMB5) gene mutation and overexpression of PSMB5 protein. *Blood* **112**, 2489–2499 (2008).

26. Levine, B. & Kroemer, G. Autophagy in the Pathogenesis of Disease. *Cell* **132**, 27–42 (2008).

27. Dikic, I. Proteasomal and Autophagic Degradation Systems. *Annu. Rev. Biochem.* **86**, 193–224 (2017).

28. Mizushima, N. & Klionsky, D. J. Protein Turnover Via Autophagy: Implications for Metabolism*. *Annu. Rev. Nutr.* **27**, 19–40 (2007).

29. Berger, Z. *et al.* Rapamycin alleviates toxicity of different aggregate-prone proteins. *Hum. Mol. Genet.* **15**, 433–442 (2006).

30. Williams, A. *et al.* Aggregate-Prone Proteins Are Cleared from the Cytosol by Autophagy: Therapeutic Implications. *Curr. Top. Dev. Biol.* **76**, 89–101 (2006).

31. Feng, Z., Zhang, H., Levine, A. J. & Jin, S. The coordinate regulation of the p53 and mTOR pathways in cells. *Proc. Natl. Acad. Sci. U. S. A.* **102**, 8204 (2005).

32. Degenhardt, K. *et al.* Autophagy promotes tumor cell survival and restricts necrosis, inflammation, and tumorigenesis. *Cancer Cell* **10**, 51 (2006).

33. Meyer, H., Bug, M. & Bremer, S. Emerging functions of the VCP/p97 AAA-ATPase in the ubiquitin system. *Nature Cell Biology* **14**, 117–123 (2012).

34. Schuberth, C. & Buchberger, A. UBX domain proteins: major regulators of the AAA ATPase Cdc48/p97. *Cell. Mol. Life Sci.* **65**, 2360–2371 (2008).

35. van den Boom, J. & Meyer, H. VCP/p97-Mediated Unfolding as a Principle in Protein Homeostasis and Signaling. *Mol. Cell* **69**, 182–194 (2018).

36. Dobrynin, G. *et al.* Cdc48/p97–Ufd1–Npl4 antagonizes Aurora B during chromosome segregation in HeLa cells. *J. Cell Sci.* **124**, 1571–1580 (2011).

37. Braun, R. J. & Zischka, H. Mechanisms of Cdc48/VCP-mediated cell death — from yeast apoptosis to human disease. *Biochim. Biophys. Acta - Mol. Cell Res.* **1783**, 1418–1435 (2008).

38. Watts, G. D. J. *et al.* Inclusion body myopathy associated with Paget disease of bone and frontotemporal dementia is caused by mutant valosin-containing protein. *Nat. Genet.* **36**, 377–381 (2004).

39. Johnson, J. O. *et al.* Exome sequencing reveals VCP mutations as a cause of familial ALS. *Neuron* **68**, 857 (2010).

40. Anderson, D. J. *et al.* Targeting the AAA ATPase p97 as an Approach to Treat Cancer through Disruption of Protein Homeostasis. *Cancer Cell* **28**, 653–665 (2015).

41. Lu, M. *et al.* Opposing unfolded-protein-response signals converge on death receptor 5 to control apoptosis. *Science* **345**, 98 (2014).

42. Zhao, Z. *et al.* CB-5083, an inhibitor of P97, suppresses osteosarcoma growth and stem cell properties by altering protein homeostasis. *Am. J. Transl. Res.* **12**, 2956 (2020).

43. A Phase 1 Study Evaluating CB-5083 in Subjects With Lymphoid Hematological Malignancies - Full Text View - ClinicalTrials.gov. Available at: https://clinicaltrials.gov/ct2/show/NCT02223598. (Accessed: 18th April 2022)

44. A Phase 1 Study Evaluating CB-5083 in Subjects With Advanced Solid Tumors - Full Text View - ClinicalTrials.gov. Available at: https://clinicaltrials.gov/ct2/show/NCT02243917. (Accessed: 18th April 2022)

45. Huryn, D. M., Kornfilt, D. J. P. & Wipf, P. P97: An Emerging Target for Cancer, Neurodegenerative Diseases, and Viral Infections. *J. Med. Chem.* **63**, 1892–1907 (2020).

46. Adams J, Palombella VJ, Sausville EA, Johnson J, Destree A, Lazarus DD, Maas J, Pien CS, Prakash S, E. P. Proteasome inhibitors: a novel class of potent and effective antitumor agents. *Cancer Research* 59(11):2615-2622 (1999).

47. Sato, Y. *et al.* Structural insights into ubiquitin recognition and Ufd1 interaction of Npl4. *Nat. Commun.* **10**, (2019).

48. Bodnar, N. O. *et al.* Structure of the Cdc48 ATPase with its ubiquitin-binding cofactor Ufd1-Npl4. *Nat. Struct. Mol. Biol.* **25**, 616 (2018).

49. Yoshino, H. *et al.* Targeting NPL4 via drug repositioning using disulfiram for the treatment of clear cell renal cell carcinoma. *PLoS One* **15**, e0236119 (2020).

50. Lu, B. S. *et al.* Upregulation of NPL4 promotes bladder cancer cell proliferation by inhibiting DXO destabilization of cyclin D1 mRNA. *Cancer Cell Int.* **19**, (2019).

51. Oliveira, J. W. de F., Rocha, H. A. O., de Medeiros, W. M. T. Q. & Silva, M. S. Application of Dithiocarbamates as Potential New Antitrypanosomatids-Drugs: Approach Chemistry, Functional and Biological. *Molecules* **24**, (2019).

52. Plyusnin, V. F., Kolomeets, A. V, Grivin, V. P., Larionov, S. V & Lemmetyinen, H. Photochemistry of Dithiocarbamate Cu(II) Complex in CCl 4. *J. Phys. Chem. A* **115**, 1763–1773 (2011).

53. Blanusa, M., Varnai, V. M., Piasek, M. & Kostial, K. Chelators as antidotes of metal toxicity: therapeutic and experimental aspects. *Curr. Med. Chem.* **12**, 2771–2794 (2005).

54. Fanjul-Bolado, P., Fogel, R., Limson, J., Purcarea, C. & Vasilescu, A. Advances in the Detection of Dithiocarbamate Fungicides: Opportunities for Biosensors. *Biosensors* **11**, (2021).

55. (EFSA), E. F. S. A. The 2017 European Union report on pesticide residues in food. *EFSA J.* **17**, (2019).

56. Kaul, L., Süss, R., Zannettino, A. & Richter, K. The revival of dithiocarbamates: from pesticides to innovative medical treatments. *iScience* **24**, (2021).

57. Eneanya, D. I., Bianchine, J. R., Duran, D. O. & Andresen, B. D. The Actions and Metabolic Fate of Disulfiram. *Annu. Rev. Pharmacol. Toxicol.* **21**, 575–596 (1981).

58. Vallari, R. C. & Pietruszko, R. Human aldehyde dehydrogenase: mechanism of inhibition of disulfiram. *Science* **216**, 637–639 (1982).

59. Kleczkowska, P., Sulejczak, D. & Zaremba, M. Advantages and disadvantages of disulfiram coadministered with popular addictive substances. *Eur. J. Pharmacol.* **904**, 174143 (2021).

60. Lipsky, J. J., Shen, M. L. & Naylor, S. In vivo inhibition of aldehyde dehydrogenase by disulfiram. *Chem. Biol. Interact.* **130**–**132**, 93–102 (2001).

61. Shen, M. L., Johnson, K. L., Mays, D. C., Lipsky, J. J. & Naylor, S. Determination of in vivo adducts of disulfiram with mitochondrial aldehyde dehydrogenase. *Biochem. Pharmacol.* **61**, 537–545 (2001).

62. Suzuki, Y. *et al.* The origin of an EPR signal observed in dithiocarbamate-loaded tissues: Copper(II)-dithiocarbamate complexes account for the narrow hyperfine lines. *Biochim. Biophys. Acta - Gen. Subj.* **1335**, 242–245 (1997).

63. Su, T. A. *et al.* A Modular Ionophore Platform for Liver-Directed Copper Supplementation in Cells and Animals. *J. Am. Chem. Soc.* **140**, 13764–13774 (2018).

64. Misra, H. P. Reaction of Copper-Zinc Superoxide Dismutase with Diethyldithiocarbamate*. *J. Biol. Chem.* **254**, 1–23 (1979).

65. Cvek, B. & Dvorak, Z. Targeting of Nuclear Factor-kB and Proteasome by Dithiocarbamate Complexes with Metals. *Curr. Pharm. Des.* **13**, 3155–3167 (2007).

66. Lövborg, H. *et al.* Inhibition of proteasome activity, nuclear factor-KB translocation and cell survival by the antialcoholism drug disulfiram. *Int. J. Cancer* **118**, 1577–1580 (2006).

67. Karin, M., Cao, Y., Greten, F. R. & Li, Z. W. NF-κB in cancer: from innocent bystander to major culprit. *Nat. Rev. Cancer* **2**, 301–310 (2002).

68. Lelièvre, P., Sancey, L., Coll, J. L., Deniaud, A. & Busser, B. The Multifaceted Roles of Copper in Cancer: A Trace Metal Element with Dysregulated Metabolism, but Also a Target or a Bullet for Therapy. *Cancers (Basel).* **12**, 1–25 (2020).

69. Skrott, Z. *et al.* Alcohol-abuse drug disulfiram targets cancer via p97 segregase adaptor NPL4. *Nature* **552**, 194–199 (2017).

70. Skrott, Z. *et al.* Disulfiram's anti-cancer activity reflects targeting NPL4, not inhibition of aldehyde dehydrogenase. *Oncogene* **38**, 6711–6722 (2019).

71. Chen, D., Cui, Q. C., Yang, H. & Dou, Q. P. Disulfiram, a clinically used anti-alcoholism drug and copper-binding agent, induces apoptotic cell death in breast cancer cultures and xenografts via inhibition of the proteasome activity. *Cancer*

Res. **66**, 10425–10433 (2006).

72. Chroma, K. *et al.* A drug repurposing strategy for overcoming human multiple myeloma resistance to standard-of-care treatment. *Cell Death Dis.* **13**, 1–11 (2022).

73. Majera, D. *et al.* Targeting the NPL4 Adaptor of p97/VCP Segregase by Disulfiram as an Emerging Cancer Vulnerability Evokes Replication Stress and DNA Damage while Silencing the ATR Pathway. *Cells* **9**, 469 (2020).

74. Reinhardt, S. *et al.* Identification of disulfiram as a secretase-modulating compound with beneficial effects on Alzheimer's disease hallmarks. *Sci. Reports 2018* **8**, 1–13 (2018).

75. Lin, M. H. *et al.* Disulfiram can inhibit MERS and SARS coronavirus papain-like proteases via different modes. *Antiviral Res.* **150**, 155 (2018).

76. Frieman, M., Ratia, K., Johnston, R. E., Mesecar, A. D. & Baric, R. S. Severe Acute Respiratory Syndrome Coronavirus Papain-Like Protease Ubiquitin-Like Domain and Catalytic Domain Regulate Antagonism of IRF3 and NF-κB Signaling. *J. Virol.* **83**, 6689 (2009).

77. Chen, T. *et al.* Synergistic Inhibition of SARS-CoV-2 Replication Using Disulfiram/Ebselen and Remdesivir. *ACS Pharmacol. Transl. Sci.* **4**, 898–907 (2021).

78. Hogarth, G. Transition Metal Dithiocarbamates: 1978–2003. *Prog. Inorg. Chem.* **53**, 71–561 (2005).

79. Kannappan, V. *et al.* Recent Advances in Repurposing Disulfiram and Disulfiram Derivatives as Copper-Dependent Anticancer Agents. *Front. Mol. Biosci.* **8**, 854 (2021).

80. Serra, R. *et al.* Disulfiram and copper combination therapy targets NPL4, cancer stem cells and extends survival in a medulloblastoma model. *PLoS One* **16**, e0251957 (2021).

81. Lomenick, B. *et al.* Target identification using drug affinity responsive target stability (DARTS). *Proc. Natl. Acad. Sci. U. S. A.* **106**, 21984–21989 (2009).

82. Genchi, G., Sinicropi, M. S., Lauria, G., Carocci, A. & Catalano, A. The Effects of Cadmium Toxicity. *Int. J. Environ. Res. Public Heal. 2020, Vol. 17, Page 3782* **17**, 3782 (2020).

83. Rini, B. I. *et al.* Pembrolizumab plus Axitinib versus Sunitinib for Advanced Renal-Cell Carcinoma. *N. Engl. J. Med.* **380**, 1116–1127 (2019).

84. Kuenzi, B. M. *et al.* Predicting Drug Response and Synergy Using a Deep Learning Model of Human Cancer Cells. *Cancer Cell* **38**, 672-684.e6 (2020).

85. Pan, M. *et al.* Seesaw conformations of Npl4 in the human p97 complex and the inhibitory mechanism of a disulfiram derivative. *Nat. Commun.* **12**, 121 (2021).

86. Xiao, Y. *et al.* Molecular study on copper-mediated tumor proteasome inhibition and cell death. *Int. J. Oncol.* **37**, 81–87 (2010).

87. Tsvetkov, P. *et al.* Copper induces cell death by targeting lipoylated TCA cycle proteins. *Science (80-.).* **375**, 1254–1261 (2022).

88. Mariotto, A. B., Enewold, L., Zhao, J., Zeruto, C. A. & Robin Yabroff, K. Medical care costs associated with cancer survivorship in the United States. *Cancer Epidemiol. Biomarkers Prev.* **29**, 1304–1312 (2020).

89. Prasad, V. & Mailankody, S. Research and Development Spending to Bring a Single Cancer Drug to Market and Revenues After Approval. *JAMA Intern. Med.* **177**, 1569 (2017).

90. Cvek, B. Nonprofit drugs as the salvation of the world's healthcare systems: The case of Antabuse (disulfiram). *Drug Discovery Today* **17**, 409–412 (2012).

91. Bill & Melinda Gates Foundation Awards $15.1 Million To Treat African Sleeping Sickness And Leishmaniasis - Bill & Melinda Gates Foundation. Available at: https://www.gatesfoundation.org/ideas/media-center/press-releases/2000/12/african-sleeping-sickness. (Accessed: 29th April 2022)